

# Discovery of the Potent and Selective MC4R Antagonist PF-07258669 for the Potential Treatment of Appetite Loss

Michelle R. Garnsey,\* Aaron C. Smith, Jana Polivkova,\* Autumn L. Arons, Guoyun Bai, Caroline Blakemore, Markus Boehm, Leanne M. Buzon, Sarah N. Campion, Matthew Cerny, Shiao-Chi Chang, Karen Coffman, Kathleen A. Farley, Kari R. Fonseca, Kristen K. Ford, Jeonifer Garren, Jimmy X. Kong, Martin R. M. Koos, Daniel W. Kung, Yajing Lian, Monica M. Li, Qifang Li, Luis A. Martinez-Alsina, Rebecca O'Connor, Kevin Ogilvie, Kiyoyuki Omoto, Brian Raymer, Matthew R. Reese, Tim Ryder, Lacey Samp, Kimberly A. Stevens, Daniel W. Widlicka, Qingyi Yang, Kaicheng Zhu, Jean-Philippe Fortin, and Matthew F. Sammons



Cite This: <https://doi.org/10.1021/acs.jmedchem.2c02012>



Read Online

ACCESS |



Metrics & More

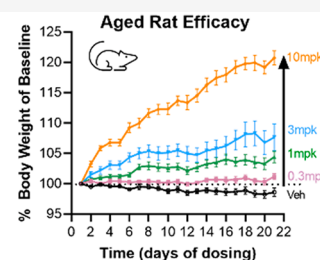
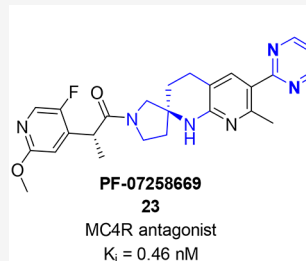


Article Recommendations



Supporting Information

**ABSTRACT:** The melanocortin-4 receptor (MC4R) is a centrally expressed, class A GPCR that plays a key role in the regulation of appetite and food intake. Deficiencies in MC4R signaling result in hyperphagia and increased body mass in humans. Antagonism of MC4R signaling has the potential to mitigate decreased appetite and body weight loss in the setting of anorexia or cachexia due to underlying disease. Herein, we report on the identification of a series of orally bioavailable, small-molecule MC4R antagonists using a focused hit identification effort and the optimization of these antagonists to provide clinical candidate **23**. Introduction of a spirocyclic conformational constraint allowed for simultaneous optimization of MC4R potency and ADME attributes while avoiding the production of hERG active metabolites observed in early series leads. Compound **23** is a potent and selective MC4R antagonist with robust efficacy in an aged rat model of cachexia and has progressed into clinical trials.



## INTRODUCTION

Melanocortin-4 receptor (MC4R) signaling in the paraventricular nucleus of the hypothalamus (PVH) plays a central role in the regulation of appetite and food intake.<sup>1</sup> MC4R is a class A G-protein-coupled receptor (GPCR) that is regulated by both endogenous MC4R agonists and inverse agonist/antagonist peptides in response to nutritional state. In states of high-energy balance, pro-opiomelanocortin (POMC) neurons release MC4R agonist peptide  $\alpha$ -melanocyte stimulating hormone ( $\alpha$ -MSH). Binding of  $\alpha$ -MSH to MC4R results in activation of MC4R signaling, suppressing appetite and food intake. In a low-energy balance state, the agouti-related peptide (AgRP) is released in the PVH. AgRP acts as a competitive antagonist of  $\alpha$ -MSH binding at MC4R and is also an MC4R inverse agonist,<sup>2,3</sup> suppressing basal MC4R signaling, leading to increased appetite and food intake.

In humans, genetic loss of MC4R signaling, either through loss of functional MC4R receptor<sup>4,5</sup> or through loss of POMC production and processing,<sup>6–8</sup> is associated with a phenotype that includes marked obesity, increased appetite and food intake, and increased body mass. Pharmacological inhibition of MC4R signaling has been proposed as a treatment for the loss of appetite and body weight associated with a number of

underlying chronic diseases.<sup>9</sup> Multiple small-molecule MC4R antagonists have been reported,<sup>10–13</sup> and the efficacy of a set of these antagonists (Figure 1) in reversing or preventing appetite or body weight loss in preclinical models of cancer, chronic kidney disease, or age-related cachexia or anorexia has been described.<sup>14–18</sup> Recent reports have described a MC4R antagonist peptide with efficacy in canine models of cachexia following oral or subcutaneous administration.<sup>19,20</sup> To the best of our knowledge, none of these previously reported small-molecule MC4R antagonists have progressed to clinical studies.

Our efforts to identify MC4R antagonist lead matter began with a focused screening campaign of approximately 28K compounds from the Pfizer compound library. These compounds were selected based on data generated during previous medicinal chemistry programs at Pfizer focused on identifying MC4R ligands.<sup>21</sup> This data was mined for

Received: December 7, 2022

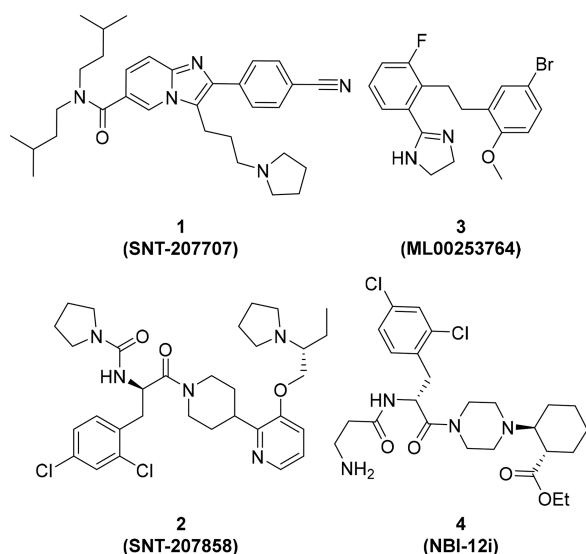
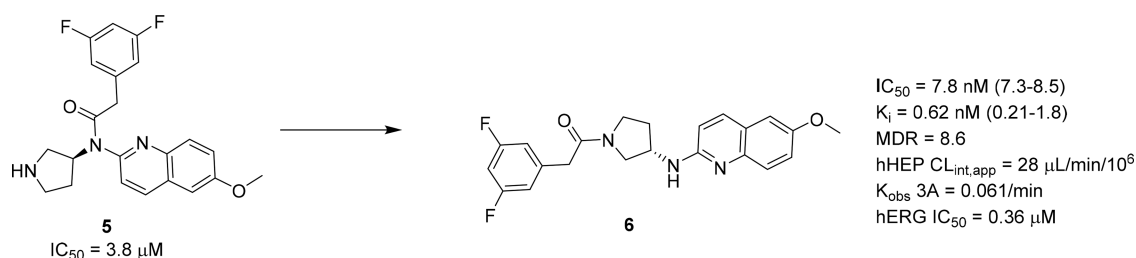


**Figure 1.** Small-molecule MC4R antagonists with reported efficacy in preclinical models.

compounds that had either demonstrated affinity for MC4R and lacked subsequent data showing MC4R agonist activity or had functional MC4R data that suggested they possessed MC4R antagonist or inverse agonist pharmacology. To minimize the likelihood of identifying MC4R partial agonists or system-dependent agonists in this screening campaign, we opted to prioritize screening in a functional MC4R inverse agonist assay.<sup>22</sup> This led to the identification of a series of putative MC4R inverse agonists represented by 3-acylaminopyrrolidine **5** (Scheme 1). While pursuing SAR studies in this series, it was observed that specific batches of these 3-acylaminopyrrolidines appeared to have time-dependent improvements in MC4R inverse agonist potency. Further investigations revealed that 3-acylaminopyrrolidine **5** undergoes an internal acyl migration to produce 1-acylaminopyrrolidine **6**.<sup>23</sup> The 1-acylaminopyrrolidine **6** is a potent MC4R inverse agonist ( $IC_{50} = 7.8$  nM) and competitive antagonist of  $\alpha$ -MSH binding at MC4R ( $K_i = 0.62$  nM), whereas the initially identified 3-acylaminopyrrolidine **5** is much less active at MC4R ( $IC_{50} = 3.8$   $\mu$ M). (The possibility that the observed weak MC4R activity of **5** is due to in situ rearrangement to produce **6** has not been ruled out.) The enantiomer of **6** was also made and tested and was 150 $\times$  less potent (see SI). Here, we report the optimization of 1-acyl-3-aminopyrrolidine MC4R ligands and the design and discovery of PF-07258669 (**23**), a potent, selective, and orally bioavailable small-molecule MC4R antagonist that is currently in Phase 1 clinical studies.

#### Scheme 1. Rearrangement of **5** via Acyl Migration To Provide MC4R-Active 1-Acylpyrrolidine **6**



## RESULTS AND DISCUSSION

Throughout the course of our medicinal chemistry program, compounds were assessed and prioritized based on their ability to competitively bind to hMC4R over the radiolabeled peptidic probe [ $^{125}$ I]NDP- $\alpha$ -MSH,<sup>24,25</sup> a modified version of the known endogenous agonist  $\alpha$ -MSH. Early leads and series representatives were also spot checked for MC4R functional inverse agonist activity in a cell-based (CHO cells) assay measuring inhibition of cyclic adenosine monophosphate (cAMP) production. While compound **6** is a potent MC4R inverse agonist, it is also a potent inhibitor ( $IC_{50} = 0.36$   $\mu$ M) of the human ether-a-go-go (hERG) potassium ion channel (product of the hERG gene; Kv11.1) and displays potent time-dependent inhibition (TDI) of cytochrome P450 3A enzymatic activity<sup>26</sup> ( $k_{obs} = 0.061$ /min, 30  $\mu$ M test concentration, Scheme 1). We hypothesized that replacing the methoxy quinoline found in **6** with a more polar functional group might improve the safety profile with respect to both TDI and hERG inhibition.<sup>27</sup> Replacement of the methoxy quinoline motif with 5-triazolo-6-methyl pyridine **7** (Figure 2) led to a slight loss of MC4R

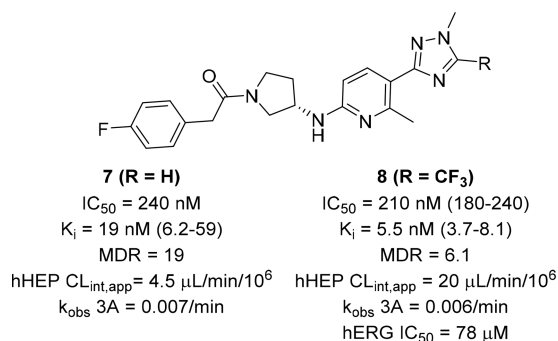


**Figure 2.** In vitro profile of analogs **7** and **8**.

potency ( $K_i = 19$  nM;  $IC_{50} = 240$  nM) relative to **6** but a significant improvement in CYP3A TDI activity ( $k_{obs} = 0.007$ /min, 30  $\mu$ M) as well as an improvement in metabolic stability in human hepatocytes<sup>28</sup> (hHEP  $CL_{int,app} = 4.5$   $\mu$ L/min/million cells vs 28  $\mu$ L/min/million cells). Although a good starting point, **7** had a high multidrug-resistance protein 1 (MDR; P-glycoprotein) efflux ratio (19), indicating that it would likely be brain impaired.<sup>29</sup> Introduction of a trifluoromethyl substituent (**8**) decreased the MDR efflux ratio relative to **7** while maintaining MC4R potency. Compound **8** had an acceptable combination of MC4R potency ( $K_i = 5.5$  nM;  $IC_{50} = 210$  nM), hHEP stability (hHEP  $CL_{int,app} = 20$   $\mu$ L/min/million cells), and MDR efflux ratio (6.1) and warranted further optimization. In addition, the hERG potency ( $IC_{50} = 78$   $\mu$ M) of **8** was also decreased relative to **6**.

Table 1. SAR of 5-Heterocyclylpyridine Series

Number	Structure	$K_i$ (nM) <sup>a</sup>	hHEP CL <sub>int,app</sub> (μL/min/million cells) <sup>b</sup>	LogD	MDR ER <sup>d</sup>
9		2.3 (0.77-7.0)	34	3.6 <sup>c</sup>	24
10		27 <sup>f</sup>	7.1	2.1 <sup>e</sup>	NT
11		1.1 (0.36-3.6)	10	2.7 <sup>e</sup>	16
12		0.77 (0.58-1.0)	15	3.4 <sup>c</sup>	6.6
13		1.2 (0.77-2.0)	15	4.2 <sup>c</sup>	6.1
14		6.4 (2.8-15)	7.9	2.6 <sup>e</sup>	4.9

<sup>a</sup>Human MC4R binding potency ( $K_i$ ) reported as the geometric mean of at least three replicates unless otherwise noted. Numbers in parentheses are the 95% confidence interval. <sup>b</sup>Apparent intrinsic clearance (CL<sub>int,app</sub>) obtained from cryopreserved human hepatocytes.<sup>28</sup> <sup>c</sup>The experimental logD using the RP-HPLC method.<sup>30,31</sup> <sup>d</sup>Efflux ratio using multidrug-resistance protein-1.<sup>32</sup> <sup>e</sup>The experimental logD using the shake-flask method at pH = 7.4.<sup>33</sup> <sup>f</sup> $f_n = 1$ .

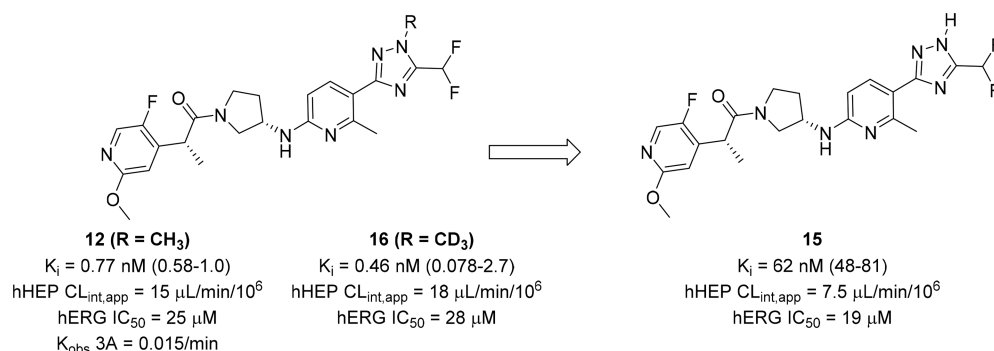


Figure 3. 12 and hERG active metabolite 15. In vitro profile of 16.

Next, the SAR of the aryl acetamide was explored to identify a compound with improved potency and properties relative to 8 (Table 1). We found that replacing the *p*-fluorophenyl with a

dimethoxyphenyl provided similar potency (9;  $K_i = 2.3$  nM) to 8 but led to an increase in hHEP turnover (hHEP CL<sub>int,app</sub> = 34 μL/min/million cells) and MDR efflux ratio (24). To reduce

hHEP turnover, we investigated whether one of the methoxy groups could be removed under the hypothesis that the two methoxy groups might not be equal in contributing to MC4R affinity. By removing one methoxy group and replacing the phenyl with 4-pyridyl **10**, the measured lipophilicity value was reduced by 1.5 log units ( $\log D = 3.6$  and  $\log D = 2.1$  for **9** and **10**, respectively).<sup>30,31</sup> Relative to **9**, the hHEP turnover of **10** was improved by nearly 5-fold (hHEP  $CL_{int,app} = 7.1 \mu\text{L}/\text{min}/\text{million cells}$ ) with some loss of MC4R potency ( $K_i = 27 \text{ nM}$ ). Introduction of a methyl alpha to the amide (**11**) significantly improves MC4R potency ( $K_i = 1.1 \text{ nM}$ ) over **10** and maintains low hHEP turnover (hHEP  $CL_{int,app} = 10 \mu\text{L}/\text{min}/\text{million cells}$ ), although with high MDR efflux ratio (16). The epimeric methyl resulted in a 1000-fold decrease in potency relative to **11** (see SI). The addition of a fluorine in **12** and **13** led to an improvement in the MDR efflux ratios (6.6 and 6.1, respectively) relative to **11** with little impact on hHEP turnover and potency. Compound **12** was selected to further characterize due to its combination of excellent potency ( $K_i = 0.77 \text{ nM}$ ), hHEP turnover (hHEP  $CL_{int,app} = 15 \mu\text{L}/\text{min}/\text{million cells}$ ), and MDR efflux ratio (6.6).

Compound **12** has a balanced MC4R potency, hHEP clearance, and MDR efflux profile, an acceptable window against hERG inhibition (hERG  $IC_{50} = 25 \mu\text{M}$ ), and reduced CYP3A TDI ( $k_{obs} = 0.015/\text{min}$ ,  $10 \mu\text{M}$ , Figure 3). However, upon analyzing the metabolite profile of **12** produced in hHEP incubations, the *N*-demethylation metabolite **15** (Figure 3) was identified and subsequently observed in circulation in vivo following oral dosing of **12** in dogs. The *N*-desmethyl metabolite **15** is more potent than the parent **12** at hERG (**12**: hERG  $IC_{50} = 25 \mu\text{M}$  vs **15**: hERG  $IC_{50} = 19 \mu\text{M}$ ), has low hHEP turnover (hHEP  $CL_{int,app} = 7.5 \mu\text{L}/\text{min}/\text{million cells}$ ), and was found to circulate in vivo in dogs at levels higher than the parent **12** (Figure 4). When taking the concentration of the parent

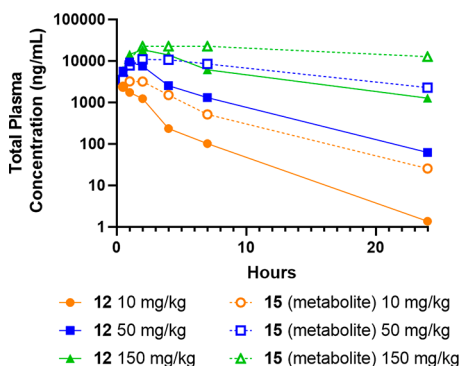


**Figure 4.** Total plasma concentrations of **12** and **15** following oral administration of **12** in dogs at 10, 50, and 150 mg/kg.

molecule **12** and its metabolite **15** into account, the margins against hERG inhibition could introduce significant risk if **12** was developed further. Therefore, efforts turned to mitigation of this metabolic liability.

We initially tried to prevent the demethylation through deuteration of the labile methyl group (**16**). While this change maintained potency ( $K_i = 0.46 \text{ nM}$ ), the demethylation metabolite **15** was still observed upon incubation of **16** with hHEP (see SI). Thus, we revisited the aryl optimization work to identify a heterocycle that would not generate this metabolite. We had previously identified **14** as an interesting lead ( $K_i = 6.4 \text{ nM}$ ) with low hHEP turnover (hHEP  $CL_{int,app} = 7.9 \mu\text{L}/\text{min}/$

million cells) and MDR efflux ratio (4.9), and we decided to explore changes to the amino pyridine motif that could further improve potency. Thus, we set out to understand the bioactive conformation of our molecules when bound to MC4R.

Our own analysis of publicly available single-crystal X-ray structures that contain a 2-alkylamino pyridine motif from the Cambridge Crystallographic Data Centre (CCDC)<sup>34</sup> (Table 2,

**Table 2.** Relative Population of the N–C–N–H Dihedral Angle for Amino Pyridine (Equilibrium A) and Quinoline (Equilibrium B)

Equilibrium A				
Equilibrium B				
equilibrium	R		trans (%)	cis (%)
A	H	CCDC <sup>a</sup>	70	30
A	H	PDB <sup>b</sup>	1.1	98.9
B	H	NMR <sup>c</sup>	79	21
		NMR <sup>d</sup>	47	53
B	H	$\Delta E^e$	0	1.02
		ratio	85	15
B	Me	$\Delta E^e$	0	4.50
		ratio	99.9	0.01

<sup>a</sup>Seventy compounds fitting this motif were pulled from the CCDC, see SI for details. <sup>b</sup>Ninety two ligands fitting this motif were pulled from the PDB, see SI for details. <sup>c</sup>From the RDC conformation of the major amide rotamer. <sup>d</sup>From the RDC conformation of the minor amide rotamer. <sup>e</sup> $\Delta E$  in kcal/mol, single-point energy was calculated in Gaussian16 with MP2/aug-cc-pVTZ with SMD implicit water solvent model. The lower energy rotamer was set as the reference with its relative energy at 0.0 kcal/mol.

equilibrium A,  $n = 70$ ) revealed that there are two preferred dihedral angles about the N–C–N–H axis (bold) that all 70 compounds displayed: either 180° (trans) or 0° (cis). Notably, the 180° (trans) dihedral angle was the predominant conformation represented with a trans:cis ratio of 70:30, suggesting that the trans conformation may be the lower energy conformation based on the observed statistics from the CCDC. The trans conformation was indeed observed in the previously reported small-molecule X-ray crystal structure of **6**.<sup>23</sup>

We next investigated the solution-phase conformation of **6** by determining the residual dipolar coupling (RDC) supported conformation by NMR spectroscopy.<sup>35–37</sup> In DMSO, **6** is an amide rotamer in a 51:49 equilibrium (see proton spectrum and NOESY spectrum in the SI). The rotamers are in slow enough exchange that we were able to observe distinct RDCs from each rotamer, which allowed us to determine the solution conformation of each rotamer independently. The major amide rotamer is 79% trans at the N–C–N–H bond. In the minor amide rotamer, the N–C–N–H bond was in a 47:53 ratio, slightly favoring the cis conformation about the N–C–N–H bond. Looking at the NOESY spectrum, interchange between



the rotamers is reasonably fast, which allows averaging of conformations between rotamers, suggesting that the trans conformation of the amino quinoline N–C–N–H bond is slightly preferred in solution (63%, Table 2, Equilibrium B). A preference for the trans conformation in solution is consistent with the CCDC analysis. Interestingly, when we queried the PDB data set for protein–ligand cocrystal structures<sup>38</sup> where the ligand contains a similar 2-aminopyridine motif, the results are starkly the opposite (Table 2, Equilibrium A,  $n = 92$ ). The dihedral distribution of those compounds from the PDB exists in the 0° (cis) conformation 98.9% of the time and is only in the 180° (trans) conformation 1.1% of the time.

On the basis of the calculated relative energy of the two conformations of 2-methylaminoquinoline (see SI for method description), the cis conformation is 1.02 kcal/mol higher in energy than the trans conformation, which correlates to an anticipated 85:15 distribution of trans to cis in solution (Table 2, Equilibrium B). This agrees with the observed distribution of 2-alkylaminopyridine conformations from the CCDC data. A similar calculation indicates an even larger energetic preference for the trans conformation when the 3 position of the quinoline ring is substituted (for example R = Me) ( $\Delta E = 4.50$  kcal/mol; 99.9:0.01 trans:cis ratio). Understanding that substitution at the 3 position of the quinoline would favor the trans conformation, we looked at data from the earlier quinoline series, where **6** and **17** (Figure 5) had been made and profiled. The potency loss

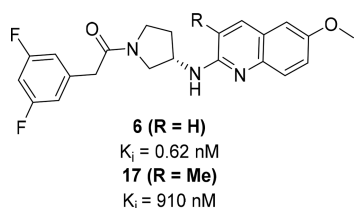


Figure 5. Binding potencies of **6** and **17**.

from R = H (**6**;  $K_i = 0.62$  nM) to R = Me (**17**;  $K_i = 910$  nM) was quite large. On the basis of these observations, we hypothesized the bioactive conformation of these molecules is the cis conformation, whereas the more populated, lower energy conformation of these 2-aminopyridine/quinoline analogs is the trans conformation.

To favor the proposed MC4R-active cis conformation, we explored locking the orientation of the ring system through spirocyclization. However, introduction of the [4.4]-spirocycle found in **18** (Table 3) resulted in a significant loss in MC4R binding potency ( $K_i$  greater than the limit of detection) relative to nonspirocyclic inhibitors such as **7**. Using the pyrrolidine ring as the overlay reference, the [4.4]-spirocycle (Figure 6, gold structure) places the amino pyridine into a different vector relative to the proposed MC4R-bioactive conformation, as shown in the yellow quinoline structure (Figure 6, yellow structure). The same structural comparison revealed that a [4.5]-spirocyclic structure (Figure 6, light blue structure) better resembles the proposed bioactive conformation. The [4.5]-spirocyclic morpholine **19** was synthesized and had improved MC4R potency (inverse agonist  $IC_{50} = 650$  nM,  $K_i$  value not obtained) relative to **18** but high MDR efflux ratio (48). [4.5]-Spiropiperidine **20** provided a drastic improvement in MC4R potency ( $K_i = 0.60$  nM;  $IC_{50} = 39$  nM) relative to **19**. Changing the 5-heterocycle from the pyrazole to the fluorinated triazoles **21** and **22** or to pyrimidine **23** provided compounds with

excellent potency, clearance, and MDR efflux ratios. The demethylation issues plaguing **12** and **13** continued to be an issue with the triazoles in the spirocyclic series, and thus, **23** was selected for further characterization based on its excellent MC4R potency ( $K_i = 0.46$  nM;  $IC_{50} = 13$  nM), hHEP turnover (hHEP  $CL_{int,app} = 12$   $\mu$ L/min/million cells), efflux ratio (4.7), and lack of observable hERG-active metabolites (Table 3). In comparison to the nonspirocyclic **14**, there is a clear improvement in MC4R binding affinity (**14**  $K_i = 6.4$  nM vs **23**  $K_i = 0.46$  nM), supporting our initial hypothesis that binding of the cis conformer is responsible for MC4R inhibition. The large improvement in potency observed upon spirocyclization may be generalizable to other 2-alkylamino pyridine motifs (e.g., hinge binders).

Further in vitro evaluation of **23** revealed a highly permeable compound ( $P_{app} = 28 \times 10^{-6}$  cm/s)<sup>39</sup> with a murine Breast Cancer Resistance Protein (mBCRP) BA/AB ratio<sup>29</sup> of 1.3. Compound **23** has a 60 000-fold window between the hERG potency ( $IC_{50} = 27$   $\mu$ M) and the MC4R binding potency with concomitant improvement over the CYP3A TDI ( $k_{obs} = 0.019$ /min (30  $\mu$ M)) from early lead **6**.

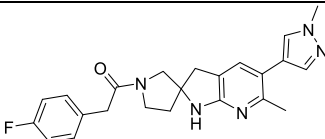
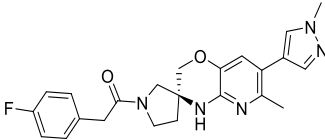
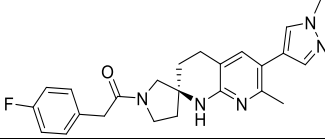
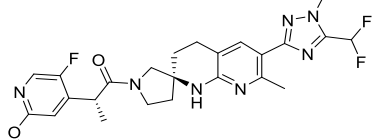
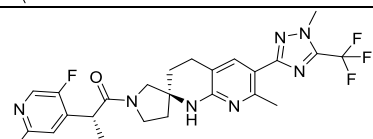
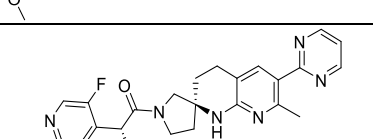
Key fragments **25a**, **25b**, **26**, and **28** were prepared as shown in Scheme 2. Dibromotriazoles **24a** and **24b** underwent selective metal–halogen exchange at the 5 position on treatment with *n*-butyllithium followed by treatment with DMF (Scheme 2a). Difluorination with Deoxo-Fluor produced difluorotriazoles **25a** and **25b**. Trifluoromethyl triazole **26** was synthesized using copper-catalyzed conditions first described by Chen and Wu.<sup>40</sup> To synthesize  $\alpha$ -methyl acid **28**, nitrile **27** was methylated with LDA and methyl iodide followed by hydrolysis (Scheme 2b).

The synthesis of analogs **7** and **9–16** is described in Scheme 3. Buchwald coupling with Boc diamine **29** and 2-chloro-6-methylpyridine led to formation of **30**. Bromination with 1,3-dibromo-5,5-dimethylhydantoin (DBDMH) followed by Ni-catalyzed coupling conditions<sup>41</sup> with tetrahydroxydiboron led to boronic acid **31**. Suzuki coupling with the desired aryl halide followed by Boc deprotection with HCl/*i*PrOH or HCl/dioxane led to formation of pyridines **32a–f**. Pyridines **32a–f** underwent amidation with the corresponding carboxylic acid to give analogs **7** and **9–16**. For phenylacetic acids with an  $\alpha$ -methyl group, careful control of reaction conditions was required to avoid epimerization. To this end, CDI with pyridinium triflate as an additive was used to reduce epimerization during coupling.<sup>42</sup>

The synthesis of analog **8** (Scheme 4) proceeded using similar disconnections as described in Scheme 3; however, amidation was implemented at the beginning of the synthesis. Amidation of Boc diamine **33** proceeded with T3P to produce **34** after Boc deprotection. Nucleophilic aromatic substitution then led to bromopyridine **35**, which was boronated and reacted in a Suzuki coupling with triazole **26** to form analog **8**.

The synthesis of the [4.4]-spirocycle **18** is described in Scheme 5. Carboxylic acid **36** was reduced with Red-Al to produce pseudobenzyl alcohol **37**. Two-step conversion of the hydroxyl group to iodide **38** proceeded by activation as the methanesulfonate followed by treatment with NaI. Alkylation with the enolate of ethyl 1-Boc-pyrrolidine-3-carboxylate followed by saponification provided **39**. Curtius rearrangement in the presence of methanol provided methyl carbamate **40**. Intramolecular Buchwald coupling proceeded with concomitant loss of the methyl carbamate to give **41**. Bromination followed by Suzuki coupling with 1-methylpyrazole-4-boronic acid pinacol ester led to formation of **42**. Boc deprotection and amidation with *p*-fluorophenyl acetic acid led to analog **18**.

Table 3. SAR of Changes to the Amino Pyrrolidine Core and Subsequent 6,6-Spiropiperidine

Number	Structure	IC <sub>50</sub> (nM) <sup>a</sup>	K <sub>i</sub> (nM) <sup>b</sup>	hHEP CL <sub>int,app</sub> (μL/min/million cells) <sup>c</sup>	LogD	MDR ER <sup>e</sup>
18 <sup>h</sup>		20,000 <sup>g</sup>	>2200	NT	1.9 <sup>d</sup>	34
19		650 (594-720)	NT	4.9	2.4 <sup>d</sup>	48
20		39 (31-48)	0.60 (0.37-0.97)	6.5	2.6 <sup>f</sup>	18
21		NT	0.49 (0.38-0.64)	11	3.2 <sup>f</sup>	8.7
22		8.4 (1.1-64)	0.45 (0.28-0.72)	12	4.0 <sup>d</sup>	4.8
23		13 (11-14)	0.46 (0.27-0.79)	12	2.6 <sup>f</sup>	4.7

<sup>a</sup>Human MC4R inverse agonist potency reported as the geometric mean of at least two replicates. Numbers in parentheses are the 95% confidence interval. <sup>b</sup>Human MC4R binding potency ( $K_i$ ) reported as the geometric mean of at least three replicates. Numbers in parentheses are the 95% confidence interval. <sup>c</sup>Apparent intrinsic clearance ( $CL_{int, app}$ ) obtained from cryopreserved human hepatocytes.<sup>28</sup> <sup>d</sup>The experimental logD using the RP-HPLC method.<sup>30,31</sup> <sup>e</sup>Efflux ratio using multidrug-resistance protein-1.<sup>32</sup> <sup>f</sup>The experimental logD using the shake-flask method at pH = 7.4.<sup>33</sup> <sup>g</sup> $n = 1$ . <sup>h</sup>Racemic.

The synthesis of spiromorpholine **19** is shown in Scheme 6. Pyrrolidine-ester **43** was acylated using LDA and ethyl chloroformate to produce diester **44**. Desymmetrization was effected through treatment with ECS-esterase **03**<sup>43</sup> to produce carboxylic acid **45** in >99% ee. Curtius rearrangement with diphenylphosphoryl azide (DPPA) and benzyl alcohol led to formation of Cbz-amine; the ester was then reduced with lithium borohydride to produce protected amino-alcohol **46**. Cyclization with thionyl chloride and subsequent oxidation with ruthenium trichloride/sodium periodate<sup>44</sup> led to sulfamate **47**. Nucleophilic attack<sup>45</sup> with 2-chloro-6-methylpyridin-3-ol in the presence of potassium carbonate led to ring opening and loss of the sulfonate to form **48**. Intramolecular Buchwald cyclization provided **49**, this was followed by bromination and Suzuki coupling as previously described and led to **50**. Boc deprotection and amidation led to analog **19**.

The synthesis of spiropiperidines **20–23** is described in Scheme 7. The previously described intermediates **38** and **46** were converted into partners **51** and **52** for a Wittig reaction

through treatment with triphenylphosphine and oxidation under Parikh–Doering conditions, respectively. Wittig coupling proceeded in the presence of potassium carbonate followed by hydrogenolysis with rhodium on alumina to provide **53** in good yield. Intramolecular cyclization under Buchwald conditions and bromination led to **54**. Boronation and Suzuki coupling with the appropriate heteroaryl halide produced **55a–d**. Boc deprotection and amidation then provided analogs **20–23**.

The in vitro functional antagonist potency of **23** was further evaluated by measuring its ability to block  $\alpha$ -MSH-induced cAMP production in a CHO cell line expressing hMC4R. The resulting  $K_b$  value for **23** at hMC4R is 0.72 nM, consistent with its hMC4R affinity ( $K_i = 0.46$  nM) determined in the [<sup>125</sup>I]NDP- $\alpha$ MSH competition binding assay (Table 3, Figure 7). Competition binding assays based on the [<sup>125</sup>I]NDP- $\alpha$ MSH probe showed that **23** retains high binding affinity at rat and dog MC4R with  $K_i$  values of 0.52 and 0.094 nM, respectively (Table S3).

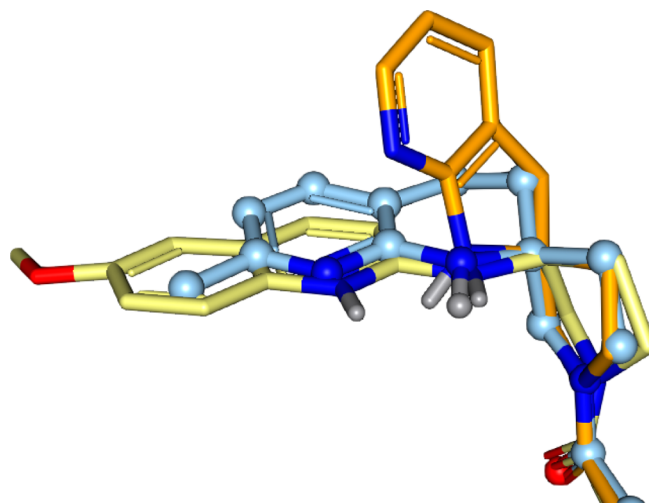
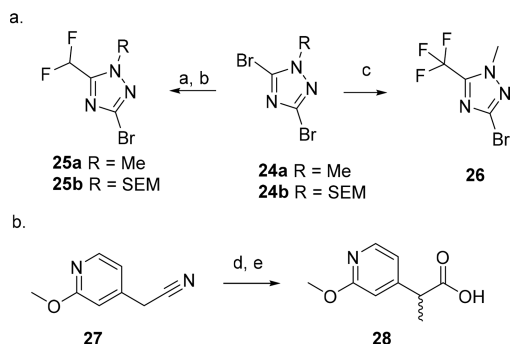


**Figure 6.** Proposed bioactive conformation of quinoline **6** (yellow) vs low-energy conformations of spirocycle **18** (gold) vs spirocycle **20** (light blue).

**Scheme 2. Synthesis of Key Intermediates: (a) Triazoles 25a, 25b, and 26 and (b) Carboxylic Acid 28**

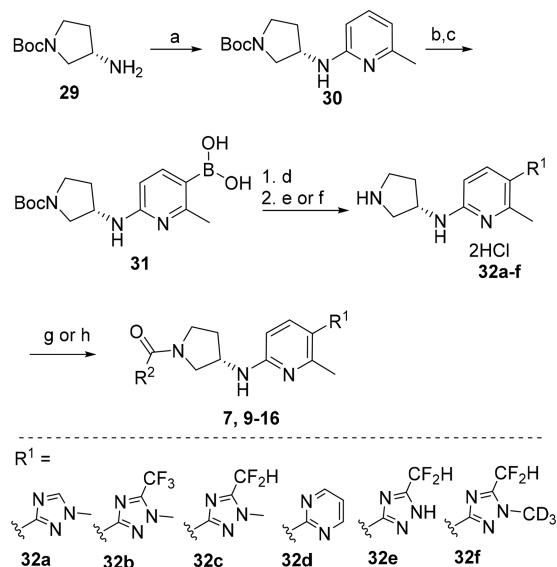


<sup>a</sup>*n*-BuLi, Et<sub>2</sub>O; then DMF, 55–63%. <sup>b</sup>Deoxo-Fluor, CH<sub>2</sub>Cl<sub>2</sub>, 53–66%. <sup>c</sup>Methyl 2,2-difluoro-2-(fluorosulfonyl)acetate, CuI, DMF, 26%. <sup>d</sup>LDA, CH<sub>3</sub>I, THF, 40%. <sup>e</sup>Aqueous NaOH, EtOH, quantitative.

The affinity of **23** against the closely related hMC1R, hMC3R, and hMC5R isoforms was determined using a competition binding assay (filtration format) using [<sup>125</sup>I]NDP- $\alpha$ MSH and membranes derived from CHO cells stably expressing either hMC1R, hMC3R, or hMC5R (Figure 7, Table S2). These studies showed that **23** binds hMC3R and hMC5R with *K<sub>i</sub>* values of 340 nM and 840 nM, respectively. Compound **23** showed weak competition binding at hMC1R with a *K<sub>i</sub>* value >1600 nM. The selectivity of **23** against other human melanocortin receptor isoforms was further evaluated using cAMP formation assays based on CHO cells stably expressing hMC1R, hMC2R, hMC3R, or hMC5R. Compound **23** does not display agonist activity at any of the four human melanocortin receptor isoforms in these assays and showed functional antagonist activity only against hMC3R (*K<sub>b</sub>* = 97 nM).

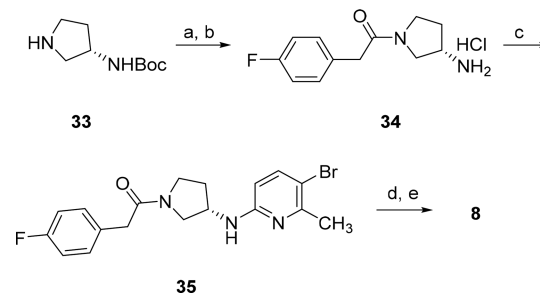
The in vivo pharmacokinetic properties of **23** were determined in rats and dogs (Table 4). Following IV administration, **23** demonstrated a total plasma clearance of 21 mL/min/kg in rats and 11 mL/min/kg in dogs with a moderate steady-state volume of distribution in both rats and dogs (*V<sub>ss</sub>* = 0.95 and 1.3 L/kg, respectively). The elimination half-life was 1 and 2.3 h in rats and dogs, respectively. Additionally, <1% of the administered dose of **23** was excreted

**Scheme 3. Synthesis of Analogs 7 and 9–16**



<sup>a</sup>2-Chloro-6-methylpyridine, Pd(OAc)<sub>2</sub>, BrettPhos, NaO-*t*-Bu, THF, 70 °C, 95%. <sup>b</sup>1,3-Dibromo-5,5-dimethylhydantoin, CH<sub>2</sub>Cl<sub>2</sub>, 10 °C, 91%. <sup>c</sup>B<sub>2</sub>(OH)<sub>4</sub>, Ni(PPh<sub>3</sub>)<sub>2</sub>Cl<sub>2</sub>, *i*-Pr<sub>2</sub>NEt, THF, CH<sub>3</sub>OH, 67%. <sup>d</sup>Representative conditions: aryl halide, Pd(PPh<sub>3</sub>)<sub>2</sub>Cl<sub>2</sub>, aq. K<sub>3</sub>PO<sub>4</sub>, THF, 70 °C, 80–96%. <sup>e</sup>AcCl, *i*PrOH, 50 °C, 71–96%. <sup>f</sup>4M HCl in dioxane, CH<sub>3</sub>OH, 99–100%. <sup>g</sup>1-2-(5-fluoro-2-methoxypyridin-4-yl)-propanoic acid, CDI, Py-TfOH, CH<sub>3</sub>CN 42–77%. <sup>h</sup>Representative conditions: carboxylic acid, *i*-Pr<sub>2</sub>NEt, HATU, CH<sub>2</sub>Cl<sub>2</sub>, 74%.

**Scheme 4. Synthesis of Analog 8**

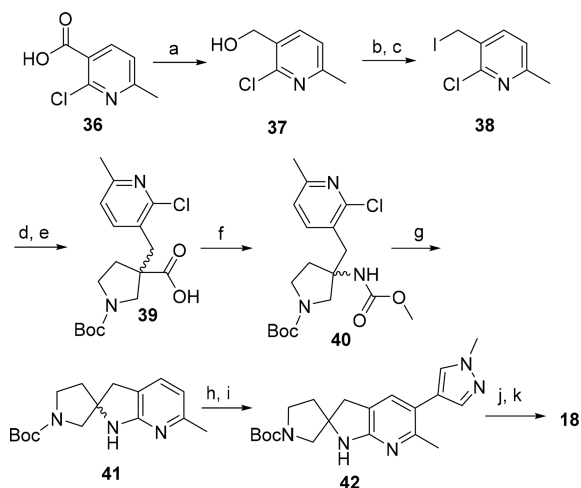


<sup>a</sup>*p*-FPhCH<sub>2</sub>CO<sub>2</sub>H, T3P (in EtOAc), *i*-Pr<sub>2</sub>NEt, CH<sub>2</sub>Cl<sub>2</sub>, 78%. <sup>b</sup>HCl (in dioxane), CH<sub>2</sub>Cl<sub>2</sub>, 96%. <sup>c</sup>3-Bromo-6-fluoro-2-methylpyridine, *i*-Pr<sub>2</sub>NEt, DMSO, 140 °C, 37%. <sup>d</sup>B<sub>2</sub>(OH)<sub>2</sub>, NiCl<sub>2</sub>(PPh<sub>3</sub>)<sub>2</sub>, *i*-Pr<sub>2</sub>NEt, THF, CH<sub>3</sub>OH, 69%. <sup>e</sup>**26**, Pd(Amphos)Cl<sub>2</sub>, KHCO<sub>3</sub>, 2-MeTHF, 80 °C, 15%.

in the urine in both species. Following oral administration of crystalline **23**, the oral bioavailability was 28% in rats and 93% in dogs. The brain penetration of **23** was evaluated in rats, the AUC-derived total brain-to-plasma ratio was 0.23, and the AUC-derived unbound brain-to-unbound plasma ratio was 0.1.

An aged rat in vivo model of geriatric anorexia<sup>46</sup> was used to assess the pharmacology and in vivo efficacy of **23**. The aged rat model is a naturalistic model that mimics a variety of physiologies and diseases associated with human aging. Key aspects of age-related anorexia are shared between rodents<sup>47–51</sup> and humans<sup>52–55</sup> including loss of appetite and body weight. The validity of the aged rat model extends beyond the replication of physiological and behavioral phenotypes, as some evidence suggests a mechanistic hypothesis that central homeostatic appetite signaling may be dysregulated in the aging rodent. Notably, in aged rats, AgRP (endogenous inverse agonist

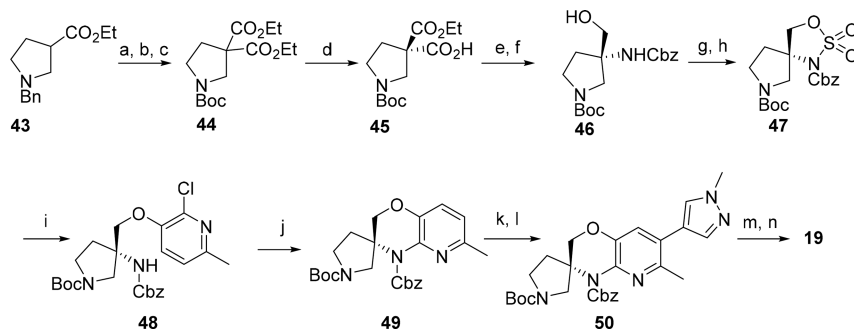
## Scheme 5. Synthesis of Analog 18



<sup>a</sup>Red-Al, PhCH<sub>3</sub>, from −5 to 5 °C, 78%. <sup>b</sup>Et<sub>3</sub>N, MsCl, PhCH<sub>3</sub>, from −5 to 5 °C. <sup>c</sup>NaI, acetone, PhCH<sub>3</sub>. <sup>d</sup>1-(*tert*-Butyl) 3-ethyl pyrrolidine-1,3-dicarboxylate, LiHMDS, THF, from 0 to 15 °C, 70%. <sup>e</sup>LiOH, CH<sub>3</sub>OH, H<sub>2</sub>O, THF, 94%. <sup>f</sup>DPPA, Et<sub>3</sub>N, CH<sub>3</sub>OH, PhCH<sub>3</sub>, 100 °C, 59%. <sup>g</sup>Pd<sub>2</sub>(dba)<sub>3</sub>, RuPhos, NaO-*t*-Bu, PhCH<sub>3</sub>, 59%. <sup>h</sup>DBDMH, CH<sub>2</sub>Cl<sub>2</sub>, CH<sub>3</sub>OH, quantitative. <sup>i</sup>1-Methylpyrazole-4-boronic acid pinacol ester, Pd(Amphos)<sub>2</sub>Cl<sub>2</sub>, KHCO<sub>3</sub>, H<sub>2</sub>O, dioxane, 90 °C. <sup>j</sup>4M HCl in dioxane, CH<sub>2</sub>Cl<sub>2</sub>, CH<sub>3</sub>OH, 85%. <sup>k</sup>*p*-FPhCH<sub>2</sub>CO<sub>2</sub>H, CDI, *i*-Pr<sub>2</sub>NEt, 2-Me-THF, DMF, 40%.

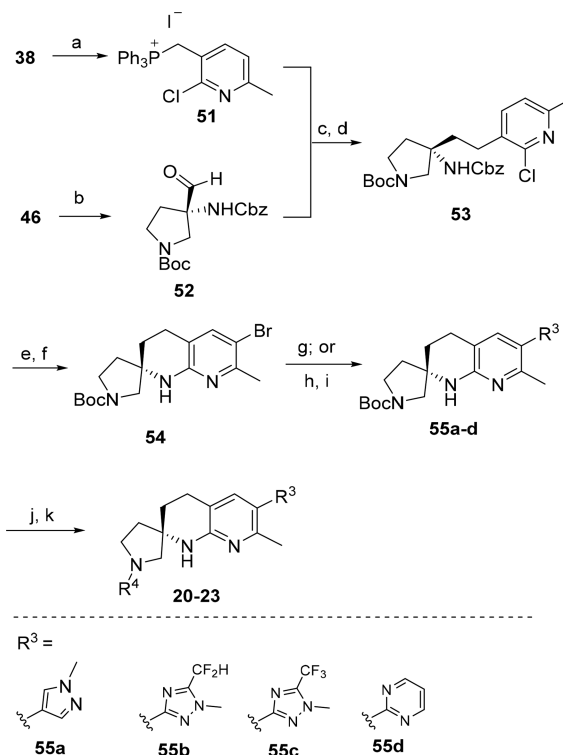
of MC4R) gene expression is lower and fails to rise appropriately in response to fasting. The aged rats' hunger response after fasting is also blunted, resulting in slower body weight recovery after caloric deficit. Despite aged rats suffering from blunted endogenous ligand release, the expression and/or signaling of MC4R itself may be pathophysiologically high in the aged animal. This is evidenced by aged animals being more sensitive to exogenous administration of AgRP or  $\alpha$ -MSH in relation to food intake and body weight compared to younger animals. Although clinical translation of this model to humans is not yet established, elderly humans show similar disturbances in feeding behavior and bodyweight gain, and thus, it is hypothesized they may suffer from dysregulation in similar hypothalamic neuro-circuits.<sup>56–61</sup> For these reasons, we believe this to be a relevant model for assessing the *in vivo* efficacy of MC4R antagonists.

## Scheme 6. Synthesis of Analog 19



<sup>a</sup>LDA, EtOC(O)Cl, THF, from −80 to −40 °C, 83%. <sup>b</sup>Pd/C, H<sub>2</sub> (50 psi), EtOH, 89%. <sup>c</sup>Boc<sub>2</sub>O, Et<sub>3</sub>N, CH<sub>2</sub>Cl<sub>2</sub>, 99%. <sup>d</sup>ECS-Esterase 03, pH 6.92 buffer, DMSO, quantitative. <sup>e</sup>DPPA, Et<sub>3</sub>N, PhCH<sub>3</sub>, from 80 to 90 °C; then BnOH, 50 °C, 57%. <sup>f</sup>LiBH<sub>4</sub>, THF, from 0 to 10 °C, 86%. <sup>g</sup>SOCl<sub>2</sub>, Pyr, CH<sub>3</sub>CN, from −40 °C to rt. <sup>h</sup>RuCl<sub>3</sub>·H<sub>2</sub>O, NaIO<sub>4</sub>, CH<sub>3</sub>CN, H<sub>2</sub>O, 64% over two steps. <sup>i</sup>2-Chloro-6-methylpyridin-3-ol, K<sub>2</sub>CO<sub>3</sub>, NMP, 80 °C, 67%. <sup>j</sup>Pd(OAc)<sub>2</sub>, RuPhos, NaO-*t*-Bu, *t*-amylOH, 94%. <sup>k</sup>NBS, CH<sub>2</sub>Cl<sub>2</sub>, 52%. <sup>l</sup>1-Methylpyrazole-4-boronic acid pinacol ester, Pd(dppf)Cl<sub>2</sub>, aq. Na<sub>2</sub>CO<sub>3</sub>, dioxane, 96%. <sup>m</sup>1.25M HCl in *i*-PrOH, 50 °C, 96%. <sup>n</sup>*p*-FPhCH<sub>2</sub>CO<sub>2</sub>H, HATU, *i*-Pr<sub>2</sub>NEt, DMF.

## Scheme 7. Synthesis of Analogs 20–23



<sup>a</sup>PPh<sub>3</sub>, CH<sub>3</sub>CN, 82%. <sup>b</sup>SO<sub>3</sub>-Pyr, Et<sub>3</sub>N, DMSO, CH<sub>2</sub>Cl<sub>2</sub>, 95%. <sup>c</sup>K<sub>2</sub>CO<sub>3</sub>, DMSO, 83%. <sup>d</sup>Rh/Al<sub>2</sub>O<sub>3</sub>, H<sub>2</sub> (30–40 psi), CH<sub>3</sub>OH, 90%. <sup>e</sup>Pd<sub>2</sub>(dba)<sub>3</sub>, RuPhos, K<sub>3</sub>PO<sub>4</sub>, PhCH<sub>3</sub>, then KOtBu, 75%. <sup>f</sup>DBDMH, EtOAc, 98%. <sup>g</sup>1-Methyl-4-(4,4,5,5-tetramethyl-1,3,2-dioxaborolan-2-yl)-1H-pyrazole, PdCl<sub>2</sub>(dppf)CH<sub>2</sub>Cl<sub>2</sub>, Na<sub>2</sub>CO<sub>3</sub>, dioxane, 62%. <sup>h</sup>Representative conditions: 5,5,5',5'-tetramethyl-2,2'-bi-1,3,2-dioxaborinane, cataCXium A, Pd(OAc)<sub>2</sub>, 2-Me-THF. <sup>i</sup>Representative conditions: aq. NaOH; 2-bromopyrimidine, Xantphos, Pd(OAc)<sub>2</sub>, toluene, 96%. <sup>j</sup>Representative conditions: 4 M HCl in dioxane, CH<sub>3</sub>OH, quantitative. <sup>k</sup>Representative conditions: (*R*)-2-(5-fluoro-2-methoxy-4-yl)propanoic acid, *i*-Pr<sub>2</sub>NEt, T3P, 2-Me-THF, 73%.

Twice-daily (BID) administration of 23 to 24–25 month old rats at 0.3, 1, 3, and 10 mg/kg led to a dose- and exposure-dependent increase in daily food intake and body weight throughout 20 days of dosing (Figure 8). An increase in cumulative food intake differentiated from the vehicle was



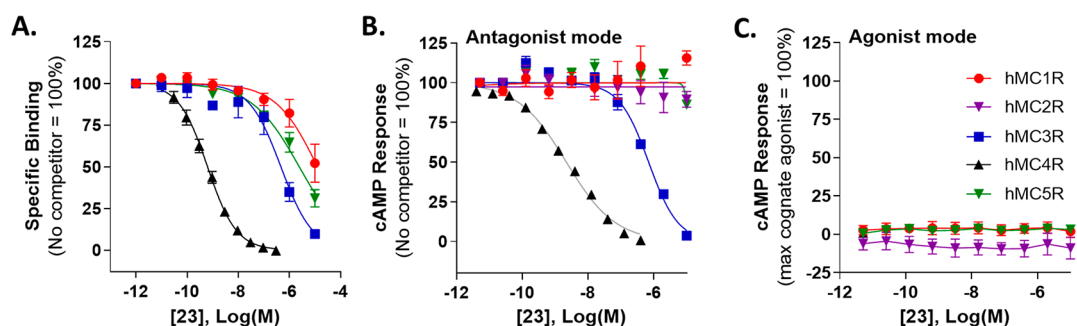


**Figure 7.** Activity of **23** at MC1R, MC2R, MC3R, MC4R, and MC5R as measured using (A) competition binding and/or (B) cAMP functional antagonist and (C) agonist mode assays. Data represents the mean  $\pm$  SEM from 3 to 22 independent experiments, each performed in triplicate (binding) or quadruplicate (cAMP).

**Table 4.** Mean Pharmacokinetics of **23** in Rats and Dogs<sup>a</sup>

species	dose (mg/kg)	route	CL <sub>p</sub> (mL/min/kg)	V <sub>ss</sub> (L/kg)	t <sub>1/2</sub> (h)	T <sub>max</sub> (h)	C <sub>max</sub> (ng/mL)	AUC <sub>inf</sub> (ng·h/mL)	AUC <sub>last</sub> (ng·h/mL)	%F <sup>b</sup>
rat	1	IV <sup>c</sup>	21	0.95	1.0			785	780	
	5	oral <sup>d</sup>			0.98	0.5	600	1120	1110	28
dog	1	IV <sup>e</sup>	11	1.3	2.3			1660	1640	
	3	oral <sup>d</sup>			3.6	0.38	1470	4610	4580	93

<sup>a</sup>Mean pharmacokinetic parameters were calculated from plasma concentration–time profiles ( $n = 2$ ). <sup>b</sup>F (%) =  $([AUC_{inf(oral)} \times dose_{(IV)}] / [AUC_{inf(IV)} \times dose_{(oral)}]) \times 100$ . <sup>c</sup>A 10% DMSO/30% PEG400/60% water formulation. <sup>d</sup>A 0.5% methylcellulose formulation. <sup>e</sup>HPBCD (23% (w/v)) in deionized water formulation.

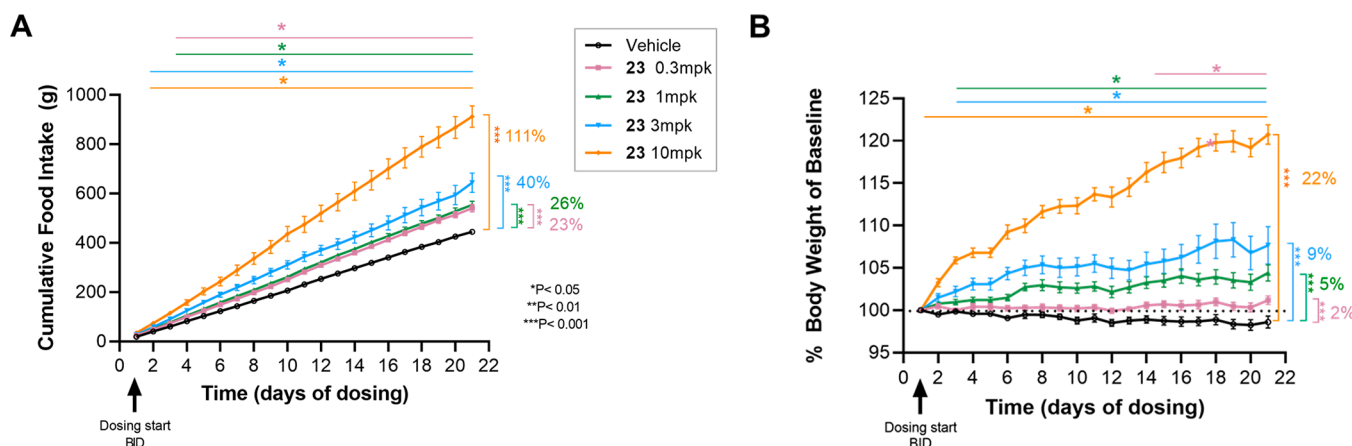


**Figure 8.** Effects of in vivo chronic BID dosing of compound **23** in an aged rat model of anorexia/cachexia at 0.3, 1, 3, and 10 mg/kg. Cumulative food intake (A) and percent bodyweight change since pretreatment baseline (B).  $n = 8$ –10/group. Mean  $\pm$  SEM. Horizontal line: earliest day to achieve statistical significance  $P < 0.05$ . Vertical brackets: effect sizes after 20 days of dosing over vehicle group; pairwise comparisons to vehicle group; annotated value represent calculated differences over vehicle group based on statistical analysis. See SI Figure S3A, In vivo Methods and Statistical Methods for details in experimental design and statistical analysis.

observed for all groups by day 3 ( $p < 0.05$ ) (Figure 8A). After 20 days of BID dosing, cumulative food intake was increased relative to vehicle-treated animals by 23%, 26%, 40%, and 111% for the 0.3, 1, 3, and 10 mg/kg groups, respectively. Cumulative body weight gains of 2%, 5%, 9%, and 22% relative to vehicle-treated animals were observed for the 0.3, 1, 3, and 10 mg/kg groups, respectively (Figure 8B).

Compound **23** was tested at a single concentration of 10  $\mu$ M in an off-target screening panel to evaluate broader pharmacological activity. The panel consisted of targets with known links to potential safety concerns and included G-protein-coupled receptors, ion channels, transporters, enzymes, and kinases (105 total targets). No activity greater than 50% of a maximal response was observed at any target tested. Additional profiling against a panel of 11 phosphodiesterase (PDE) enzyme subtypes was conducted to reveal no activity less than 50  $\mu$ M. The

potency of **23** was also tested against the ion channels Na<sub>v</sub>1.5 ( $>100$   $\mu$ M) and Ca<sub>v</sub>1.2 ( $>100$   $\mu$ M). Compound **23** was profiled at the hERG (K<sub>v</sub>11.1) ion channel and was found to inhibit the current at this channel in a patch clamp experiment with an IC<sub>50</sub> value of 27  $\mu$ M. It is not anticipated that such activity would have any physiological consequences at clinically relevant exposures.

The nonclinical safety profile of **23** was evaluated in vivo in rats and dogs. The rats and dogs were chosen as the nonclinical species because there is high sequence homology between rat, dog, and human MC4R (see SI),<sup>62,63</sup> the in vitro binding affinity of **23** to rat and dog MC4R was confirmed and is similar across species, and rats demonstrate the pharmacological effect of increased food consumption and body weight gain. Exploratory toxicology studies were completed with **23** over 14 days of dosing in Wistar Han rats and 8 days of dosing in Beagle dogs, and there were no development limiting safety or tolerability

findings in either species. Increased food consumption and body weight gain were observed in both the male and the female rats, consistent with the expected pharmacology.

## CONCLUSIONS

In summary, highly potent and selective MC4R antagonists were identified starting from the methoxy quinoline-based lead **6**. Early lead optimization focused on improving safety concerns related to hERG and TDI liabilities, which led us away from the lipophilic and hERG-active methoxy quinoline leads in favor of a new 5-heterocyclic pyridine series with better aligned ADME and safety profiles. From this optimization work, **12** was identified as a selective and potent MC4R antagonist, but an unexpectedly hERG-active *N*-demethylation metabolite led to deprioritization of **12** and related analogs. 5-Pyrimidyl-pyridine analog **14** was identified as an analog of interest, absent of metabolic liabilities but lacking the necessary potency. Thus, an effort to lock the *cis*-bioactive conformation was undertaken, in which a spirocyclization strategy was discovered, leading to the eventual discovery of clinical candidate **23**. The results of this work suggest the potential for a general strategy to improve potency of other 2-aminopyridine compounds through this spirocyclization approach. Compound **23** was further profiled to reveal a potent and selective MC4R antagonist with a greatly reduced hERG liability from early leads and an acceptable PK profile in preclinical species. The *in vitro* CYP3A TDI liability was also reduced compared to early leads, and the TDI risk will be further evaluated in early clinical trials. Compound **23** showed robust *in vivo* efficacy in an aged rat model of geriatric anorexia and proceeded through both rat and dog nonclinical safety studies without any development limiting safety or tolerability findings. The safety, tolerability, pharmacokinetics, pharmacodynamics, and CYP3A TDI risk of **23** are currently being evaluated in single-dose and multiple-dose Phase 1 clinical trials<sup>64</sup> in healthy adult participants.

## EXPERIMENTAL SECTION

**General Experimental Methods.** All chemicals, reagents, and solvents were purchased from commercial sources and were used without further purification. <sup>1</sup>H NMR data are reported relative to residual solvent signals and are reported as follows: chemical shift (ppm), multiplicity, coupling constant (Hz), and integration. The multiplicities are denoted as follows: s, singlet; d, doublet; t, triplet; q, quartet; m, multiplet; br s, broad singlet. Silica gel chromatography was performed using Biotage or ISCO purification systems with prepackaged columns. Concentration under reduced pressure was performed on a rotary evaporator with a water bath temperature not exceeding 60 °C. Purity of final compounds was assessed by HPLC with UV detection at 215 nm; all tested compounds were >95% purity. All animal studies conducted were reviewed and approved by Pfizer Institutional Animal Care and Use Committee with experimental details in the Supporting Information.

**Synthesis of 23.** *Synthesis of (2-Chloro-6-methylpyridin-3-yl)methanol (37).* Sodium bis(2-methoxyethoxy)aluminum hydride solution (Red-Al, 70%; 1.05 kg, 2.5 equiv) was added to a −5 to 5 °C solution of 2-chloro-6-methylpyridine-3-carboxylic acid (**36**, 250 g, 1.46 mol) in toluene (2.5 L). After the reaction mixture had been stirred at from −5 to 5 °C for 19 h, it was treated with a solution of sodium hydroxide (145.7 g, 3.642 mol) in water (1.25 L) while the internal temperature was maintained below 0 to 10 °C. The resulting mixture was then warmed to 25 °C; after 15 min, the aqueous layer was extracted with isopropyl acetate (2 × 1.25 L). These two extracts were combined with the toluene layer and filtered through silica gel (125 g). The filter cake was rinsed with isopropyl acetate (125 mL), and the combined filtrates were concentrated to 8 volumes at a temperature of

40–45 °C, affording **37** as a solution in toluene (1.602 kg, 11.2% by weight); the bulk of this solution was used in the following step. Estimated yield: 179.4 g, 1.138 mol, 78%. <sup>1</sup>H NMR (400 MHz, DMSO-*d*<sub>6</sub>) δ: 7.81 (d, *J* = 7.8 Hz, 1H), 7.29 (d, *J* = 7.7 Hz, 1H), 5.48 (t, *J* = 5.6 Hz, 1H), 4.50 (d, *J* = 5.6 Hz, 2H), 2.43 (s, 3H). HPLC: 95.1%.

*Synthesis of 2-Chloro-3-(iodomethyl)-6-methylpyridine (38).* *Step 1: (2-Chloro-6-methylpyridin-3-yl)methylmethanesulfonate.* Triethylamine (134.2 g, 1.326 mol) was added to a solution of **37** in toluene (from the previous step; 1.537 kg, 11.2% by weight, 172.1 g, 1.09 mol). The solution was cooled to from −5 to 5 °C and then treated in a dropwise manner with methanesulfonyl chloride (128.5 g, 1.122 mol) while maintaining the internal temperature at from −5 to 5 °C. After the reaction mixture had been stirred at this temperature for 2 h, triethylamine (22.7 g, 0.224 mol) was again added followed by dropwise addition of methanesulfonyl chloride (25.7 g, 0.224 mol). Stirring was continued at from −5 to 5 °C for 1 h, whereupon the reaction mixture was treated with water (800 mL), while the internal temperature was maintained below 25 °C and then stirred for 15 min at 25 °C. The organic layer was washed with water (805 mL) and concentrated to provide (2-chloro-6-methylpyridin-3-yl)-methylmethanesulfonate as a solution in toluene (861 g). This solution was used directly in the following step. <sup>1</sup>H NMR (400 MHz, DMSO-*d*<sub>6</sub>) δ: 7.92 (d, *J* = 7.7 Hz, 1H), 7.36 (d, *J* = 7.7 Hz, 1H), 5.30 (s, 2H), 3.29 (s, 3H), 2.48 (s, 3H).

*Step 2: 2-Chloro-3-(iodomethyl)-6-methylpyridine (38).* Sodium iodide (230 g, 1.53 mol) was dissolved in acetone (1.13 kg) at 25 °C; to this solution was added a solution of (2-chloro-6-methylpyridin-3-yl)methylmethanesulfonate in toluene (from the previous step; 861 g, ≤1.09 mol). After the reaction mixture had been stirred at 25 °C for 1 h, a solution of sodium metabisulfite (57.86 g, 0.3044 mol) in water (1.45 L) was added and stirring was continued for 30 min. The organic layer was separated, diluted with toluene (420 mL), and concentrated to 5 volumes, providing **38** as a solution in toluene (1.110 kg, 22.93% by weight). This solution was used directly for the synthesis of **51**. Estimated yield: 254.5 g, 0.9514 mol, 87% over 2 steps. <sup>1</sup>H NMR (400 MHz, DMSO-*d*<sub>6</sub>) δ: 7.90 (d, *J* = 7.7 Hz, 1H), 7.26 (d, *J* = 7.8 Hz, 1H), 4.55 (s, 2H), 2.41 (s, 3H). HPLC: 95.2%. Note: A separate batch was prepared using the same conditions on smaller scale, isolated, and taken forward to synthesize **39**.

*Synthesis of [(2-Chloro-6-methylpyridin-3-yl)methyl](triphenyl)phosphonium iodide (51).* A solution of **38** in toluene (vide supra; 1.110 kg, 22.93% by weight, 254.5 g, 0.9514 mol) was diluted with acetonitrile (1.29 L) and treated with triphenylphosphine (262 g, 0.999 mol). After the reaction mixture had been stirred for 4 h at 25 °C, it was cooled to 10 °C, stirred at that temperature for 16 h, and filtered. The filter cake was washed with toluene (255 mL) and dried at 45 °C for 4 h, affording **51** (412.6 g, 56% over four steps) as a solid. <sup>1</sup>H NMR (400 MHz, DMSO-*d*<sub>6</sub>) δ: 7.97–7.90 (m, 3H), 7.80–7.71 (m, 8H), 7.71–7.66 (m, 4H), 7.44 (dd, *J* = 7.8, 2.4 Hz, 1H), 7.20 (d, *J* = 7.8 Hz, 1H), 5.15 (d, *J*<sub>HP</sub> = 15.0 Hz, 2H), 2.40 (d, *J* = 2.4 Hz, 3H). HPLC: 99.7%.

*Synthesis of 1-tert-Butyl 3,3-Diethyl Pyrrolidine-1,3,3-tricarboxylate (44).* *Step 1: Diethyl 1-Benzylpyrrolidine-3,3-dicarboxylate.* A solution of ethyl 1-benzylpyrrolidine-3-carboxylate (700 g, 3.00 mol) in tetrahydrofuran (4.20 L) was added in a dropwise manner over 5 h to a solution of lithium diisopropylamide (2.0 M, 2.40 L, 4.80 mol) from −80 to −70 °C. Stirring was continued at from −80 to −70 °C for 2 h, whereupon ethyl chloroformate (423.5 g, 3.90 mol) was added over 3 h, while the reaction temperature was maintained at from −80 to −70 °C. After the reaction mixture had been stirred for 2 h at from −80 to −70 °C, the temperature was adjusted to from −50 to −40 °C, and the reaction was quenched by addition of a solution of acetic acid (288 g, 4.80 mol) in tetrahydrofuran (1.40 L), while the temperature was kept at from −50 to −40 °C. The resulting mixture was warmed to 15–25 °C and partitioned between water (3.50 L) and 2-methyltetrahydrofuran (7.0 L). After this mixture had been stirred for 30 min at 15–25 °C, the aqueous layer was extracted with 2-methyltetrahydrofuran (7.0 L), and the combined organic layers were washed with a solution of acetic acid (288 g, 4.80 mol) in water (4.2 L) and then with an aqueous solution of sodium sulfate (10%; 2 × 3.50 kg). The organic layers were concentrated *in vacuo* to 2–3 volumes while keeping the temperature

below 50 °C. Ethanol (4.90 L, 7 volumes) was added, and the solution was again concentrated in vacuo to 2–3 volumes while keeping the temperature below 50 °C. This ethanol addition/concentration was carried out a total of three times, with the final round employing 2.80 L of ethanol, followed by concentration to 4–5 volumes. This provided diethyl 1-benzylpyrrolidine-3,3-dicarboxylate as a solution in ethanol (3.148 kg, 24.23% by weight). A portion of this solution was used in the following step. Estimated yield: 762.8 g, 2.498 mol, 83%. A sample was isolated for characterization: <sup>1</sup>H NMR (400 MHz, DMSO-*d*<sub>6</sub>) δ: 7.35–7.20 (m, 5H), 4.12 (q, *J* = 7.1 Hz, 4H), 3.57 (s, 2H), 2.90 (s, 2H), 2.55 (t, *J* = 6.9 Hz, 2H), 2.29 (t, *J* = 6.8 Hz, 2H), 1.14 (t, *J* = 7.1 Hz, 6H).

**Step 2: Diethyl Pyrrolidine-3,3-dicarboxylate, L-Tartrate Salt.** Ethanol (720 mL, 6 volumes) was added to a solution of diethyl 1-benzylpyrrolidine-3,3-dicarboxylate (120 g, 0.393 mol) in ethanol (from the previous step; approximately 500 mL). After addition of wet palladium on carbon (10%; 12 g), the reaction vessel was evacuated and charged with argon three times and then evacuated and charged with hydrogen three times. Hydrogenation was then carried out at 40–50 psi and 40–50 °C for 24 h. The resulting mixture was filtered through diatomaceous earth (50 g); the filter cake was washed with ethanol (240 mL, 2 volumes), and the combined filtrates were concentrated in vacuo to 2.5–3.5 volumes while keeping the temperature at or below 45 °C. This solution was added, over 2 h, to a 40–50 °C solution of L-tartaric acid (76.7 g, 0.511 mol) in water (85 mL, 0.7 volumes) and ethanol (465 mL). After the mixture had been stirred at 40–50 °C for 1 h, a seed of diethyl pyrrolidine-3,3-dicarboxylate, L-tartrate salt (0.4 g; see below) was added at 45 °C. The mixture was cooled to 10 °C over 6 h and then stirred at 10 °C for 4 h; filtration provided a filter cake, which was washed with ethanol (2 volumes) and dried at 40 °C for 20 h to afford diethyl pyrrolidine-3,3-dicarboxylate, L-tartrate salt (127.4 g, 89%) as a solid. HPLC purity: 99.1%. <sup>1</sup>H NMR (400 MHz, DMSO-*d*<sub>6</sub>) δ: 4.16 (q, *J* = 7.1 Hz, 4H), 4.03 (s, 2H), 3.49 (s, 2H), 3.08 (t, *J* = 7.1 Hz, 2H), 2.32 (t, *J* = 7.1 Hz, 2H), 1.18 (t, *J* = 7.1 Hz, 6H).

The seed material used above was obtained from another run of the same synthesis of diethyl pyrrolidine-3,3-dicarboxylate, L-tartrate salt, in which solid formed directly upon cooling.

**Step 3: 1-tert-Butyl 3,3-Diethyl Pyrrolidine-1,3,3-tricarboxylate (44).** Di-tert-butyl dicarbonate (19.7 g, 90.3 mmol) was added in a dropwise manner to a 20–30 °C mixture of diethyl pyrrolidine-3,3-dicarboxylate, L-tartrate salt (88.12 g, 0.2412 mol) and triethylamine (73.33 g, 0.7247 mol) in dichloromethane (881 mL). Additional di-tert-butyl dicarbonate (19.2 g, 88.0 mmol and 19.3 g, 88.4 mmol) was added dropwise after periodic HPLC analysis. After the reaction mixture had been stirred at 20–30 °C for 18 h, the pH was adjusted to 7 by addition of hydrochloric acid (1 M; 309 g), and stirring was continued for 15 min. The organic layer was stirred with aqueous sodium sulfate solution (10%; 485.30 g) at 20–30 °C for 15 min, and then the organic layer was concentrated in vacuo to 1–2 volumes while the temperature was maintained below 40 °C. Dimethyl sulfoxide (71.7 g) was added to afford **44** as a solution in dimethyl sulfoxide (154.2 g, 48.9% by weight). The bulk of this material was progressed to the following step. Estimated yield: 75.4 g, 0.239 mol, 99%. A sample was isolated for characterization. <sup>1</sup>H NMR (400 MHz, DMSO-*d*<sub>6</sub>) δ: 4.16 (q, *J* = 7.1 Hz, 4H), 3.67 (br s, 2H), 3.34–3.26 (m, 2H), 2.37–2.28 (m, 2H), 1.39 (s, 9H), 1.17 (br t, *J* = 7.1 Hz, 6H). HPLC: 97.7%.

**Synthesis of (3R)-1-(tert-Butoxycarbonyl)-3-(ethoxycarbonyl)-pyrrolidine-3-carboxylic Acid (45).** ECS-Esterase 03 enzyme [*Bacillus stearothermophilus*, recombinant from *Escherichia coli*, (EC 3.1.1.1); 0.540 g] was added to phosphate buffer (0.1 M; pH = 6.92, 580 mL, 8.2 volumes) at 20–30 °C. A solution of **44** (72.2 g, 0.229 mol) in dimethyl sulfoxide (from the previous step; approximately 148 g) was added; additional dimethyl sulfoxide (9 mL) was used to rinse the initial vessel, and this was also added to the reaction mixture. The initial reaction pH was 7.08; after stirring at 20–30 °C for 1 h, the pH decreased to 6.58. A pH autotitrator was used to maintain the pH at 7.5 by addition of an aqueous sodium hydroxide solution (2 M; 121 mL, 0.242 mol) over 24 h. Hydrochloric acid (6 M; 52 mL, 0.312 mol) was added, bringing the pH to 2.39; ethyl acetate (435 mL, 6.0 volumes) was then added, and the mixture was stirred for 30 min at 20–30 °C. Filtration through diatomaceous earth (18.0 g) provided a filter cake, which was rinsed

with ethyl acetate (2 × 75 mL). The combined filtrates were stirred at 20–30 °C for 30 min, and then, the aqueous layer was stirred with ethyl acetate (217 mL, 3.0 volumes) for 30 min. The combined organic layers were washed twice with water (360 mL, 5.0 volumes) by stirring for 30 min. The resulting solution was concentrated in vacuo to 1–2 volumes while maintaining the temperature below 40 °C; then, it was diluted with toluene (360 mL). This concentration/dilution procedure was carried out a total of three times, providing **45** as a solution in toluene (418.3 g, 15.67% **39** by weight). Estimated yield: 65.6 g, 0.228 mol, quantitative. A sample was isolated for characterization. <sup>1</sup>H NMR (400 MHz, CDCl<sub>3</sub>) δ: 7.99 (v br s, 1H), 4.22 (q, *J* = 7.1 Hz, 2H), [3.88 (br s) and 3.83 (br s), total 2H], 3.51–3.38 (m, 2H), 2.41 (t, *J* = 7.1 Hz, 2H), 1.44 (s, 9H), 1.26 (br t, *J* = 7 Hz, 3H).

**Synthesis of tert-Butyl (3S)-3-[[[(benzyloxy)carbonyl]amino]-3-(hydroxymethyl)pyrrolidine-1-carboxylate (46).** **Step 1: 1-tert-Butyl 3-Ethyl (3S)-3-[[[(benzyloxy)carbonyl]amino]pyrrolidine-1,3-dicarboxylate.** Toluene (170 mL, 1.2 volumes) was added to a solution of **45** in toluene (3.8 volumes, containing 28.9% by weight of **39**, 146.4 g, 0.5096 mol); the solution was heated to 80–90 °C. To this was slowly added, over 2 h, a mixture of triethylamine (77.4 g, 0.765 mol) and diphenyl phosphorazidate (140.3 g, 0.5098 mol) in toluene (732 mL, 5 volumes). The reaction mixture was stirred at 80–90 °C for 3 h, whereupon it was cooled to 50 °C and treated dropwise, over 2 h, with a solution of benzyl alcohol (55.12 g, 0.5097 mol) in toluene (290 mL, 2 volumes). After the reaction mixture had been stirred at 100 °C for 16 h, it was cooled to 15–25 °C and partitioned between toluene (1.46 L, 10 volumes) and water (2.20 L, 15 volumes) by stirring for 30 min. The organic layer was washed sequentially with aqueous potassium carbonate solution (10%; 3 × 1.46 L) and with water (2 × 750 mL). It was then concentrated in vacuo to 1–2 volumes while the temperature was maintained below 50 °C, and it was diluted with tetrahydrofuran (1.0 L). This concentration/dilution procedure was carried out a total of three times, whereupon the mixture was concentrated in vacuo to 4–5 volumes while maintaining the temperature below 50 °C. This afforded 1-tert-butyl 3-ethyl (3S)-3-[[[(benzyloxy)carbonyl]amino]pyrrolidine-1,3-dicarboxylate as a solution in tetrahydrofuran (595.8 g, 19.14% by weight). Estimated yield: 114 g, 0.290 mol, 57%. A small amount was isolated for characterization. <sup>1</sup>H NMR (400 MHz, CDCl<sub>3</sub>) δ: 7.40–7.28 (m, 5H), 5.25 (v br s, 1H), 5.10 (br s, 2H), 4.28–4.12 (m, 2H), 3.91–3.76 (m, 1H), 3.71–3.38 (m, 3H), 2.54–2.15 (m, 2H), 1.45 (s, 9H), 1.27–1.16 (m, 3H).

**Step 2: tert-Butyl (3S)-3-[[[(benzyloxy)carbonyl]amino]-3-(hydroxymethyl)pyrrolidine-1-carboxylate (46).** A solution of lithium borohydride in tetrahydrofuran (2 M; 511 mL, 1.02 mol) was added over 2 h to a 0–10 °C solution of 1-tert-butyl 3-ethyl (3S)-3-[[[(benzyloxy)carbonyl]amino]pyrrolidine-1,3-dicarboxylate in tetrahydrofuran (835.6 g, containing 19.20% by weight, 160.4 g, 0.4087 mol). After the reaction mixture had been stirred at 0–10 °C for 15 h, it was cooled to from –5 to 5 °C and treated in a dropwise manner with hydrochloric acid (0.5 M; 2.08 L, 1.04 mol, 13 volumes) to a pH of 7. The mixture was then warmed to 20–30 °C, diluted with ethyl acetate (1.60 L, 10 volumes), and stirred for 10 min, whereupon the organic layer was concentrated in vacuo to 2–3 volumes while maintaining the temperature at or below 50 °C. The resulting mixture was diluted with acetonitrile (880 mL) and concentrated in vacuo to 2–3 volumes while maintaining the temperature at or below 50 °C; this dilution/concentration procedure was carried out a total of three times. The mixture was then heated to 40–50 °C and stirred for 1 h, whereupon it was cooled over 4 h to 15–25 °C. Water (164 mL) was added dropwise over 2 h at 15–25 °C, and the mixture was stirred at 15–25 °C for 12 h. The resulting solid was collected via filtration and dried in vacuo for 40 h at a temperature at or below 50 °C to afford **46** (123.2 g, 86%) as a solid. <sup>1</sup>H NMR (400 MHz, DMSO-*d*<sub>6</sub>) δ: 7.40–7.27 (m, 5H), 4.99 (s, 2H), 4.93 (t, *J* = 5.8 Hz, 1H), 3.58–3.45 (m, 3H), 3.31–3.21 (m, 3H), 2.10–1.85 (m, 2H), 1.38 (s, 9H). HPLC purity: 99.8%. Note: A separate batch was prepared using the same conditions on a smaller scale, isolated, and taken forward to synthesize **47**.

**Synthesis of tert-Butyl (3S)-3-[[[(benzyloxy)carbonyl]amino]-3-formylpyrrolidine-1-carboxylate (52).** A solution of **46** (125 g, 0.357 mol) and dimethyl sulfoxide (144.5 g, 1.849 mol) in



dichloromethane (2.02 L) was stirred for 2 h at 35–45 °C; Karl Fischer analysis indicated a water content of 0.029%. The solution was concentrated in vacuo to 3–4 volumes at 35–45 °C and then diluted with dichloromethane (1.80 L). Another Karl Fischer analysis revealed a water content of 0.034%. The solution was concentrated in vacuo at 35–45 °C to 6–7 volumes, whereupon triethylamine (112.3 g, 1.110 mol) was added at 20–30 °C, and the reaction mixture was cooled to from –5 to 0 °C and stirred at that temperature for 15 min. Sulfur trioxide pyridine complex (141.3 g, 0.8878 mol) was added in portions over 2 h; stirring was then continued at from –5 to 0 °C for 16 h, at which time the reaction mixture was warmed to 35–45 °C and concentrated to 2–3 volumes. After the mixture had cooled to 20–30 °C, it was partitioned between ethyl acetate (945 mL) and water (675 mL), and the aqueous layer was extracted with ethyl acetate (675 mL). The combined organic layers were washed sequentially with hydrochloric acid (1 M; 675 mL), water (675 mL), and saturated aqueous sodium bicarbonate solution (675 mL) and then concentrated to dryness at 30–40 °C, providing **52** (118.7 g, 95%) as an oil. HPLC purity: 91.2%. <sup>1</sup>H NMR (400 MHz, CDCl<sub>3</sub>) δ: 9.59 (s, 1H), 7.42–7.29 (m, 5H), 5.39 (br s, 1H), 5.12 (s, 2H), 3.85–3.70 (m, 1H), 3.63–3.43 (m, 3H), 2.44–2.04 (m, 2H), 1.45 (s, 9H).

**Synthesis of tert-Butyl (3S)-3-[(Benzyloxy)carbonyl]amino-3-[2-(2-chloro-6-methylpyridin-3-yl)ethyl]pyrrolidine-1-carboxylate (53).** Step 1: *tert-Butyl (3R)-3-[(Benzyloxy)carbonyl]amino-3-[2-(2-chloro-6-methylpyridin-3-yl)ethyl]pyrrolidine-1-carboxylate*. A mixture of **52** (237.1 g, 0.6805 mol) and **51** (393.6 g, 0.7429 mol) in dimethyl sulfoxide (2.40 L, 10 volumes) was treated with potassium carbonate (188.7 g, 1.365 mol) and heated at 60 °C for 2 h. Isopropyl acetate (1.54 L, 6.5 volumes), water (6.40 L, 27 volumes), and aqueous sodium sulfate solution (10%; 710 mL, 3.0 volumes) were then added, and the mixture was stirred for 20 min at 25 °C. The organic layer was washed three times with an aqueous sodium sulfate solution (10%; 1.30 L, 5.5 volumes) by stirring each mixture for 20 min before separation. It was then washed with aqueous sodium bicarbonate solution (7%; 1.30 L, 5.5 volumes) in the same manner and concentrated in vacuo to 1–2 volumes at a temperature at or below 50 °C. Isopropyl acetate (1.06 L) was added, and the mixture was concentrated in vacuo to 1–2 volumes at a temperature at or below 50 °C. Isopropyl acetate (480 mL) was added, followed by dropwise addition of methylcyclohexane (1.66 L) at 20–30 °C. After the resulting mixture had been stirred at 20–30 °C for 1 h, it was cooled to from –15 to –5 °C and stirred at that temperature for 16 h. Filtration of the slurry was carried out at from –15 to –5 °C, and the filter cake was washed with a mixture of isopropyl acetate and methylcyclohexane (3:7 ratio, 710 mL) at from –15 to –5 °C. The combined filtrates were concentrated in vacuo, diluted with methylcyclohexane (20 volumes), and subjected to silica gel chromatography (gradient: 14% to 25% ethyl acetate in methylcyclohexane) to afford *tert*-butyl (3R)-3-[(benzyloxy)carbonyl]amino-3-[2-(2-chloro-6-methylpyridin-3-yl)ethyl]pyrrolidine-1-carboxylate as a mixture of *E/Z* isomers (268.1 g, 83%) and an oil. This material was judged by <sup>1</sup>H NMR analysis to consist of 3–4 isomers/rotamers. <sup>1</sup>H NMR (400 MHz, DMSO-*d*<sub>6</sub>) characteristic peaks: δ: 8.00 (d, *J* = 7.9 Hz) and 7.59 (d, *J* = 7.6 Hz), total 1H], [7.85 (s) and 7.41 (s), total 1H], [7.38–7.25 (m), 7.22 (br d, *J* = 7.2 Hz), and 7.16 (d, *J* = 7.7 Hz), total 6H], [6.62 (d, component of AB quartet, *J* = 16.1 Hz) and 6.34 (d, *J* = 12.3 Hz), total 1H], [6.49 (br d, component of AB quartet, *J* = 16.0 Hz), 5.88 (d, *J* = 12.3 Hz), and 5.87 (d, *J* = 12.3 Hz), total 1H], [5.04 (AB quartet, *J*<sub>AB</sub> = 12.7 Hz, *J*<sub>AB</sub> = 16.4 Hz), 4.74 (d, component of AB quartet, *J* = 12.4 Hz), and 4.70–4.62 (m), total 2H], 3.83–3.68 (m, 1H), 3.32–3.16 (m, 3H), [2.43 (s) and 2.36 (s), total 3H], 2.27–2.12 (m, 1H), 2.00–1.85 (m, 1H), [1.40 (s), 1.39 (s), 1.37 (s), and 1.34 (s), total 9H]. HPLC purity: ≥99.7%.

**Step 2: *tert*-Butyl (3S)-3-[(Benzyloxy)carbonyl]amino-3-[2-(2-chloro-6-methylpyridin-3-yl)ethyl]pyrrolidine-1-carboxylate (53).** A reaction vessel containing *tert*-butyl (3R)-3-[(benzyloxy)carbonyl]amino-3-[2-(2-chloro-6-methylpyridin-3-yl)ethyl]pyrrolidine-1-carboxylate (283.0 g, 0.5996 mol) and rhodium on alumina (5%; 14.15 g) in methanol (1.98 L) was evacuated and charged with argon three times and then evacuated and charged with hydrogen three times. Hydrogenation was then carried out for 40 h at 30–40 psi and 20–25

°C. After the reaction mixture had been filtered through diatomaceous earth (424 g), the filter cake was washed with methanol (5 volumes); the combined filtrates were concentrated in vacuo at 35–45 °C. The resulting material was treated with toluene (5 volumes) and concentrated in vacuo at 50–60 °C; this toluene addition/concentration procedure was carried out a total of three times, providing **53** (254.4 g, 90%). <sup>1</sup>H NMR (400 MHz, CDCl<sub>3</sub>) δ: 7.41–7.28 (m, 6H), 6.99 (br d, *J* = 7.6 Hz, 1H), 5.06 (s, 2H), 4.91–4.79 (m, 1H), 3.62 (d, *J* = 11.7 Hz, 1H), 3.57–3.36 (m, 2H), 3.36–3.26 (m, 1H), 2.74–2.55 (m, 2H), 2.48 (s, 3H), [2.48–2.40 (m), 2.39–2.07 (m) and 2.05–1.82 (m), total 4H], 1.45 (br s, 9H). HPLC purity: 97.1%.

**Synthesis of *tert*-Butyl (2S)-6-Bromo-7-methyl-3,4-dihydro-1H-spiro[1,8-naphthyridine-2,3'-pyrrolidine]-1'-carboxylate (54).** Step 1: *tert*-Butyl (2S)-7-Methyl-3,4-dihydro-1H-spiro[1,8-naphthyridine-2,3'-pyrrolidine]-1'-carboxylate. A solution of **53** in toluene (947.73 g, containing 19% by weight, 180 g, 0.380 mol) was diluted with toluene (1.17 L, 6.5 volumes) and treated sequentially with 2-dicyclohexylphosphino-2',6'-diisopropoxybiphenyl (RuPhos; 35.44 g, 75.95 mmol) and potassium phosphate (145.1 g, 0.6836 mol). The resulting mixture was purged three times with nitrogen, whereupon tris-(dibenzylideneacetone)dipalladium(0) (34.78 g, 37.98 mmol) was added, and three additional rounds of purging with nitrogen were carried out. The reaction mixture was stirred for 24 h at 75–85 °C. Potassium phosphate (16.2 g, 0.117 mol) was added, and stirring was continued at 75–85 °C for an additional 16 h. After the reaction mixture had been cooled to 20–30 °C, potassium *tert*-butoxide (76.7 g, 0.684 mol) was added, and the reaction mixture was stirred for 2 h at 75–85 °C. It was then cooled and partitioned between water (2.25 L) and ethyl acetate (2.25 L); after being stirred for 30 min at 20–30 °C, the mixture was filtered through diatomaceous earth (180 g) and the filter cake was washed with ethyl acetate (1.80 L). The organic layer of the combined filtrates was washed sequentially with water (2 × 2.25 L) and aqueous sodium sulfate solution (10%; 2.25 L) and then extracted three times with aqueous citric acid solution (0.5 M; 1.072 kg, 1.4 equiv). The combined citric acid layers were washed with ethyl acetate (2 × 1.07 L) and then adjusted to pH 7 by addition of an aqueous sodium hydroxide solution (30%; 596 g) at 20–30 °C. Extraction of the aqueous layer with ethyl acetate (3 × 1.07 L) followed by combination of these three organic layers provided *tert*-butyl (2S)-7-methyl-3,4-dihydro-1H-spiro[1,8-naphthyridine-2,3'-pyrrolidine]-1'-carboxylate (86.9 g, 75%) as a solution in ethyl acetate (3.218 kg, 2.7% by weight). The bulk of this material was progressed to the following step. <sup>1</sup>H NMR (400 MHz, CDCl<sub>3</sub>) δ: 7.11 (d, *J* = 7.3 Hz, 1H), 6.41 (d, *J* = 7.4 Hz, 1H), 4.90 (br s, 1H), 3.59–3.43 (m, 2H), [3.40 (d, component of AB quartet, *J* = 11.1 Hz) and 3.36–3.25 (m), total 2H], 2.80–2.65 (m, 2H), 2.31 (s, 3H), 2.00–1.75 (m, 4H), [1.45 (s) and 1.44 (s), total 9H]. HPLC purity: 98.9%.

**Step 2: *tert*-Butyl (2S)-6-Bromo-7-methyl-3,4-dihydro-1H-spiro[1,8-naphthyridine-2,3'-pyrrolidine]-1'-carboxylate (54).** 1,3-Dibromo-5,5-dimethylimidazolidine-2,4-dione (45.60 g, 0.1595 mol) was added to a 0–5 °C solution of *tert*-butyl (2S)-7-methyl-3,4-dihydro-1H-spiro[1,8-naphthyridine-2,3'-pyrrolidine]-1'-carboxylate in ethyl acetate (from the previous step; 2986 g, containing 2.7% by weight, 80.6 g, 0.266 mol). After the reaction mixture had been stirred for 1 h at 0–5 °C, it was quenched by addition of an aqueous sodium sulfite solution (10%; 203 g) and water (456 mL), and the resulting mixture was stirred at 10–20 °C for 20 min. The aqueous layer was extracted twice with ethyl acetate (415 mL, 5.1 volumes) by stirring at 10–20 °C for 20 min; the combined organic layers were then stirred for 20 min with an aqueous sodium sulfate solution (10%; 456 g). Concentration of the organic layer to 1–2 volumes in vacuo below 50 °C was followed by dilution with methanol (480 mL, 6 volumes). This concentration/dilution procedure was carried out a total of three times, and the final solution was concentrated in vacuo, below 50 °C, to 5–6 volumes. The resulting solution was cooled to 15–25 °C, water (415 mL) was slowly added over 2 h at 15–25 °C, and then stirring was carried out for 14 h at 15–25 °C. Filtration provided a filter cake, which was washed with a mixture of methanol and water (1:1, 2 × 200 mL) and then dried under vacuum at 45 °C for 48 h to afford **54** (99.50 g, 98%) as a solid. LCMS



calcd for  $C_{17}H_{24}BrN_3O_2$   $[M + H]^+$ : 382.1, 384.1. Found: 384.1 (bromine isotope pattern observed).  $^1H$  NMR (400 MHz, DMSO- $d_6$ )  $\delta$ : 7.37 (s, 1H), 7.03–6.97 (m, 1H), 3.55–3.43 (m, 1H), 3.3–3.25 (m, 1H, assumed; partially obscured by water peak), 3.24–3.13 (m, 2H), 2.75–2.55 (m, 2H), 2.30 (s, 3H), 1.95–1.77 (m, 2H), 1.76–1.59 (m, 2H), 1.40 (s) and 1.38 (s), total 9H]. HPLC purity: 99.7%.

**Synthesis of tert-Butyl (2S)-7-Methyl-6-(pyrimidin-2-yl)-3,4-dihydro-1H-spiro[1,8-naphthyridine-2,3'-pyrrolidine]-1'-carboxylate (55d).** Step 1: tert-Butyl (2S)-6-(5,5-Dimethyl-1,3,2-dioxaborinan-2-yl)-7-methyl-3,4-dihydro-1H-spiro[1,8-naphthyridine-2,3'-pyrrolidine]-1'-carboxylate. Di(1-adamantyl)-*n*-butylphosphine (cata-CXium A; 2.21 g, 6.16 mmol) followed by palladium(II) acetate (0.461 mg, 2.05 mmol) were added to 2-methyltetrahydrofuran (170 mL); the catalyst mixture was sparged with argon for 10–20 min between each manipulation. The mixture was heated at reflux for 1 h and then cooled to  $\leq 50^\circ C$ . In a separate reactor, **54** (98.2% by mass; 80.0 g, 205 mmol), 5,5,5',5'-tetramethyl-2,2'-bi-1,3,2-dioxaborinane (60.3 g, 267 mmol), potassium acetate (97% by mass; 62.4 g, 617 mmol), and water (2.37 mL, 132 mmol) were added to 2-methyltetrahydrofuran (220 mL). The sides of the reactor were rinsed with 2-methyltetrahydrofuran (100 mL), and the resulting mixture was sparged with argon for approximately 1 h. The catalyst mixture was then added via cannula over less than 2 min, and the reaction mixture was heated to reflux at a rate of  $1^\circ C/min$ . After 4 h at reflux, it was cooled to  $10^\circ C$ , held at that temperature overnight, and rapidly treated dropwise over 15 min with an aqueous sodium hydroxide solution (1.0 M; 410 mL, 410 mmol). The internal temperature was maintained below  $17^\circ C$  during the addition. The resulting mixture was warmed to  $20^\circ C$ , diluted with tert-butyl methyl ether (180 mL), and mixed well for 5 min, whereupon the aqueous layer was confirmed to be at pH 10. To the organic layer was added aqueous sodium hydroxide solution (1.0 M; 480 mL, 480 mmol) in four portions over 4 min; after stirring for 5 min, the organic layer was separated and similarly extracted with an aqueous sodium hydroxide solution (1.0 M; 480 mL, 480 mmol). The combined sodium hydroxide extracts were mixed with toluene (240 mL) and treated portionwise with hydrochloric acid (12.2 M; 62.3 mL, 760 mmol) at a rate that maintained the temperature below  $30^\circ C$ . The pH of the resulting mixture was 14; additional hydrochloric acid (12.2 M; 34 mL, 415 mmol) was added to adjust the pH to 10. After the mixture had been stirred for 5 min, the aqueous layer was extracted with toluene ( $2 \times 240$  mL), and the toluene layers were combined, affording tert-butyl (2S)-6-(5,5-dimethyl-1,3,2-dioxaborinan-2-yl)-7-methyl-3,4-dihydro-1H-spiro[1,8-naphthyridine-2,3'-pyrrolidine]-1'-carboxylate as a solution in toluene. The bulk of this material was used in the following step. Estimated yield: 73.2 g (by quantitative NMR), 176 mmol, 86% yield.

**Step 2: tert-Butyl (2S)-7-Methyl-6-(pyrimidin-2-yl)-3,4-dihydro-1H-spiro[1,8-naphthyridine-2,3'-pyrrolidine]-1'-carboxylate (55d).** To a solution of tert-butyl (2S)-6-(5,5-dimethyl-1,3,2-dioxaborinan-2-yl)-7-methyl-3,4-dihydro-1H-spiro[1,8-naphthyridine-2,3'-pyrrolidine]-1'-carboxylate in toluene (from the previous step; 509 mL, containing 72.7 g, 175 mmol) were added an aqueous sodium hydroxide solution (1 M; 530 mL, 530 mmol) followed by 2-bromopyrimidine (39.0 g, 245 mmol). The resulting mixture was sparged with argon for 30 min, whereupon 4,5-bis-(diphenylphosphino)-9,9-dimethylxanthene (Xantphos; 1.27 g, 2.19 mmol) and palladium(II) acetate (394 mg, 1.76 mmol) were added. After the reaction mixture had been heated at  $50^\circ C$  for 3.5 h, it was cooled to  $20^\circ C$ , allowed to stir overnight, and filtered. The filter cake was rinsed with toluene (150 mL), and the organic layer of the combined filtrates was washed with water by stirring for 5 min and then allowing the mixture to stand for 30 min; solids in the mixture were kept with the organic layer, which was subjected to short-path distillation at 100 mbar and  $60^\circ C$ . The mixture was distilled until approximately 275 mL remained, whereupon it was cooled to  $20^\circ C$  at a rate of  $1^\circ C/min$ . After the mixture had stirred for 30 min, during which time solids were noted, heptane (727 mL) was slowly added dropwise, over 30 min. The resulting solution was stirred for 10 min, heated to  $60^\circ C$  at a rate of  $1^\circ C/min$ , and stirred at  $60^\circ C$  for 90 min, whereupon it was cooled to  $20^\circ C$  at a rate of  $1^\circ C/min$  and allowed to stir for 3 days. Filtration,

followed by rinsing of the solid cake twice with the filtrate and once with heptane (220 mL) provided **55d** (63.85 g, 96%) as a solid. HPLC purity: 99.4%.  $^1H$  NMR (600 MHz, DMSO- $d_6$ )  $\delta$ : 8.80 (d,  $J = 4.8$  Hz, 2H), 7.90 (s, 1H), 7.27 (t,  $J = 4.8$  Hz, 1H), [7.25 (br s) and 7.24 (br s), total 1H], 3.56–3.49 (m, 1H), 3.37–3.30 (m, 1H), 3.28–3.21 (m, 2H), 2.80–2.73 (m, 1H), 2.73–2.65 (m, 1H), 2.59 (s, 3H), 1.99–1.84 (m, 2H), 1.82–1.69 (m, 2H), [1.41 (s) and 1.39 (s), total 9H].

**Synthesis of (2R)-2-(5-Fluoro-2-methoxypyridin-4-yl)-1-[(2S)-7-methyl-6-(pyrimidin-2-yl)-3,4-dihydro-1H-spiro[1,8-naphthyridine-2,3'-pyrrolidine]-1'-yl]propan-1-one (23).** Step 1: (2S)-7-Methyl-6-(pyrimidin-2-yl)-3,4-dihydro-1H-spiro[1,8-naphthyridine-2,3'-pyrrolidine]. A solution of **55d** (96% by mass; 50.0 g, 126 mmol) in water (100 mL) and 2-propanol (150 mL) was added over 10 min to an  $80^\circ C$  mixture of water (150 mL) and concentrated sulfuric acid (14.5 mL, 272 mmol). After the reaction mixture had been stirred at  $80^\circ C$  for 4 h, it was cooled to  $25^\circ C$  and was then subjected to short-path distillation at  $120^\circ C$  and atmospheric pressure. When the mixture had been distilled to a volume of approximately 200 mL, the temperature was lowered to  $50^\circ C$ , activated carbon (Darco G-60; 10 g) was added, and stirring was continued for 1.5 h at  $50^\circ C$ . The mixture was then cooled to  $25^\circ C$  and filtered using a  $10\ \mu m$  filter. The filter cake was rinsed with water (100 mL), and the combined filtrates were diluted with 2-propanol (20 mL); the resulting mixture, of pH 0.86, was basified to the point of haziness that then cleared up by addition of a 6 M aqueous sodium hydroxide solution (approximately 75 mL). The resulting pH was 9.32. The mixture was treated dropwise with additional 6 M aqueous sodium hydroxide solution (approximately 20 drops) to a pH of 9.6–9.7, at which point haziness persisted. Stirring was continued for 45 min, whereupon additional 6 M aqueous sodium hydroxide solution (to a total of approximately 80 mL, 480 mmol) was added, and stirring was continued at  $20^\circ C$  for 30 min. The mixture was then heated to  $50^\circ C$  at a rate of  $1^\circ C/min$ , stirred for 1.5 h, and cooled to  $20^\circ C$  at a rate of  $1^\circ C/min$ . After stirring for 1.5 h, the mixture was filtered; the filter cake was rinsed with an aqueous sodium hydroxide solution (1 M; 100 mL, 100 mmol), and dried overnight in vacuo at  $50^\circ C$  to provide (2S)-7-methyl-6-(pyrimidin-2-yl)-3,4-dihydro-1H-spiro[1,8-naphthyridine-2,3'-pyrrolidine]. Yield: 30.87 g, 98.1% via quantitative NMR, 108 mmol, 86%.  $^1H$  NMR (600 MHz, DMSO- $d_6$ )  $\delta$ : 8.79 (d,  $J = 4.8$  Hz, 2H), 7.88 (s, 1H), 7.25 (t,  $J = 4.8$  Hz, 1H), 7.01 (s, 1H), 2.99 (ddd,  $J = 11.0, 8.4, 6.4$  Hz, 1H), 2.79 (ddd,  $J = 10.9, 8.6, 5.6$  Hz, 1H), 2.75–2.68 (m, 3H), 2.61 (d,  $J = 11.3$  Hz, 1H), 2.58 (s, 3H), 1.80–1.68 (m, 3H), 1.65 (ddd,  $J = 12.7, 8.6, 6.4$  Hz, 1H).

**Step 2: (2R)-2-(5-Fluoro-2-methoxypyridin-4-yl)-1-[(2S)-7-methyl-6-(pyrimidin-2-yl)-3,4-dihydro-1H-spiro[1,8-naphthyridine-2,3'-pyrrolidine]-1'-yl]propan-1-one (23).** A slurry of (R)-2-(5-fluoro-2-methoxypyridin-4-yl)propanoic acid (19.1 g, 95.9 mmol) in 2-methyltetrahydrofuran (200 mL) was treated with (2S)-7-methyl-6-(pyrimidin-2-yl)-3,4-dihydro-1H-spiro[1,8-naphthyridine-2,3'-pyrrolidine] (98.1% by mass, 25 g, 87.2 mmol) followed by *N,N*-diisopropylethylamine (19 mL, 110 mmol). 2,4,6-Tripropyl-1,3,5,2,4,6-trioxatriphosphinane 2,4,6-trioxide (50% solution by weight in ethyl acetate; 65 mL, 110 mmol) was added over 15 min at a rate that maintained the internal reaction temperature below  $30^\circ C$ . After the reaction mixture had been stirred for 100 min, an aqueous sodium bicarbonate solution (1.14 M; 250 mL, 285 mmol) was added {Caution: gas evolution}, and stirring was continued for 10 min at  $20^\circ C$ . The resulting mixture was heated to  $40^\circ C$ , stirred for 30 min, and again treated with an aqueous sodium bicarbonate solution (1.14 M; 125 mL, 142 mmol). After this mixture had been stirred for 80 min, water (75 mL) was added and stirring was continued for 10 min. The organic layer was subjected to distillation at  $60^\circ C$  and 500 mbar until the mixture had been reduced to 5 volumes. 2-Methyltetrahydrofuran (125 mL) was added, the temperature was adjusted to  $45$ – $50^\circ C$ , and the mixture was filtered through diatomaceous earth. Additional 2-methyltetrahydrofuran (50 mL) was used to rinse the filter pad, and the combined filtrates were distilled at  $60^\circ C$  and 500 mbar to approximately 3 volumes. The heat was increased to  $80^\circ C$  until solids at the bottom of the reactor were released and then decreased to  $50^\circ C$ . The resulting material was treated at  $50^\circ C$  over 15 min with heptane (250 mL) and allowed to stir at  $50^\circ C$  for 90 min. It was then cooled to  $20^\circ C$  at a rate

of 1 °C/min and allowed to stir for 3 days, whereupon it was diluted to a volume of 600 mL by addition of 10 mol % 2-methyltetrahydrofuran in heptane. Filtration provided a filter cake, which was rinsed with heptane (75 mL) and dried overnight at 50 °C in vacuo, affording **23** (29.63 g, 64.06 mmol, 73%) as a solid. HPLC purity: 100%. LCMS calcd for  $C_{25}H_{27}FN_6O_2$   $[M + H]^+$ : 463.3. Found:  $m/z$  463.3  $[M + H]^+$ .  $^1H$  NMR (500 MHz, DMSO)  $\delta$ : 8.80 (d,  $J$  = 4.8 Hz, 2H), 8.79 (d,  $J$  = 4.9 Hz, 2H), 8.11 (d,  $J$  = 1.5 Hz, 1H), 8.09 (d,  $J$  = 1.5 Hz, 1H), 7.88 (s, 1H), 7.86 (s, 1H), 7.35 (s, 1H), 7.26 (t,  $J$  = 4.9 Hz, 1H), 7.26 (t,  $J$  = 4.3 Hz, 1H), 7.25 (m, 1H), 6.75 (d,  $J$  = 4.9 Hz, 1H), 6.69 (d,  $J$  = 4.9 Hz, 1H), 4.14 (q,  $J$  = 6.9 Hz, 1H), 4.09 (q,  $J$  = 7.0 Hz, 1H), 3.82 (s, 3H), 3.81 (s, 3H), 3.73 (dt,  $J$  = 10.1, 7.5 Hz, 1H), 3.58 (ddd,  $J$  = 11.6, 7.8, 6.2 Hz, 1H), 3.53 (d,  $J$  = 10.5 Hz, 1H), 3.52 (m, 1H), 3.44 (t,  $J$  = 8.3 Hz, 1H), 3.41 (d,  $J$  = 12.1 Hz, 1H), 3.31 (d,  $J$  = 12.1 Hz, 1H), 3.25 (d,  $J$  = 10.3 Hz, 1H), 2.73 (m, 2H), 2.67 (m, 1H), 2.58 (s, 3H), 2.57 (s, 3H), 2.46 (dt,  $J$  = 16.4, 6.6 Hz, 1H), 1.98 (m, 1H), 1.95 (s, 2H), 1.83 (m, 1H), 1.78 (m, 2H), 1.62 (t,  $J$  = 6.6 Hz, 2H), 1.33 (d,  $J$  = 6.3 Hz, 3H), 1.32 (d,  $J$  = 6.6 Hz, 3H). Two rotamers were observed at approximately 1:0.8 relative concentration; exchange between them was confirmed by NOESY experiment.  $^{13}C$  NMR (126 MHz, DMSO)  $\delta$ : 169.66, 169.65, 165.50, 165.49, 160.19 (d,  $J$  = 1.1 Hz), 160.12 (d,  $J$  = 1.4 Hz), 156.92, 156.91, 154.94, 154.85, 154.67, 154.62, 153.28 (d,  $J$  = 243.4 Hz), 153.26 (d,  $J$  = 243.4 Hz), 141.17 (d,  $J$  = 16.1 Hz), 140.98 (d,  $J$  = 16.1 Hz), 138.07, 138.05, 132.90 (d,  $J$  = 27.3 Hz), 132.83 (d,  $J$  = 27.6 Hz), 121.15, 121.08, 117.75, 117.72, 111.59, 111.46, 109.63 (d,  $J$  = 1.8 Hz), 109.41 (d,  $J$  = 1.8 Hz), 59.19, 57.49, 56.77, 56.48, 53.53, 53.48, 44.15, 43.89, 37.29, 36.47, 35.53, 35.50, 29.13, 28.51, 24.36, 24.28, 23.00, 22.75, 17.58, 17.01. Multiplets stem from  $^{19}F$ ,  $^{13}C$  coupling; two rotamers were observed.  $^{19}F$  NMR (564 MHz, DMSO)  $\delta$ : -144.94 (d,  $J$  = 5.1 Hz), -144.96 (d,  $J$  = 5.4 Hz). Multiplets stem from  $^1H$ ,  $^{19}F$  coupling; two rotamers were observed. HRMS calcd for  $C_{25}H_{27}FN_6O_2$   $[M + H]^+$ : 463.3. Found: 463.2248.

## ■ ASSOCIATED CONTENT

### SI Supporting Information

The Supporting Information is available free of charge at <https://pubs.acs.org/doi/10.1021/acs.jmedchem.2c02012>.

Experimental data for compounds **8–22**; copies of NMR spectra for compounds **12** and **23**, full NMR assignment for **23**, copies of HPLC traces for **8**, **11–13**, **15**, **16**, **18**, and **20–23**; experimental information for all in vitro and in vivo experiments, metabolite identification studies for **12**; MC4R sequence alignment across species; details of the CCDC and PDB queries; off-target safety penal for **23**; single-crystal X-ray information for **23**; full NMR and RDC data for **6** (PDF)

Molecular formula strings for compounds **6–23** and associated data (CSV)

Coordinates for the small molecule crystal structure of **23** (CIF)

## ■ AUTHOR INFORMATION

### Corresponding Authors

Michelle R. Garnsey – Pfizer, Incorporated, Cambridge, Massachusetts 02139, United States; [orcid.org/0000-0003-1226-1868](https://orcid.org/0000-0003-1226-1868); Email: [michelle.garnsey@pfizer.com](mailto:michelle.garnsey@pfizer.com)

Jana Polivkova – Pfizer, Incorporated, Groton, Connecticut 06340, United States; Email: [jana.polivkova@pfizer.com](mailto:jana.polivkova@pfizer.com)

### Authors

Aaron C. Smith – Pfizer, Incorporated, Groton, Connecticut 06340, United States; [orcid.org/0000-0001-6796-5155](https://orcid.org/0000-0001-6796-5155)

Autumn L. Arons – Pfizer, Incorporated, Cambridge, Massachusetts 02139, United States

Guoyun Bai – Pfizer, Incorporated, Groton, Connecticut 06340, United States

Caroline Blakemore – Pfizer, Incorporated, Groton, Connecticut 06340, United States; [orcid.org/0000-0001-7055-6379](https://orcid.org/0000-0001-7055-6379)

Markus Boehm – Pfizer, Incorporated, Cambridge, Massachusetts 02139, United States; [orcid.org/0000-0002-7025-3287](https://orcid.org/0000-0002-7025-3287)

Leanne M. Buzon – Pfizer, Incorporated, Groton, Connecticut 06340, United States

Sarah N. Campion – Pfizer, Incorporated, Groton, Connecticut 06340, United States

Matthew Cerny – Pfizer, Incorporated, Groton, Connecticut 06340, United States

Shiao-Chi Chang – Pfizer, Incorporated, Cambridge, Massachusetts 02139, United States

Karen Coffman – Pfizer, Incorporated, Groton, Connecticut 06340, United States

Kathleen A. Farley – Pfizer, Incorporated, Groton, Connecticut 06340, United States; [orcid.org/0000-0001-8935-6852](https://orcid.org/0000-0001-8935-6852)

Kari R. Fonseca – Pfizer, Incorporated, Cambridge, Massachusetts 02139, United States

Kristen K. Ford – Pfizer, Incorporated, Groton, Connecticut 06340, United States

Jeonifer Garren – Pfizer, Incorporated, Cambridge, Massachusetts 02139, United States

Jimmy X. Kong – Pfizer, Incorporated, Cambridge, Massachusetts 02139, United States

Martin R. M. Koos – Pfizer, Incorporated, Groton, Connecticut 06340, United States; [orcid.org/0000-0002-7829-4729](https://orcid.org/0000-0002-7829-4729)

Daniel W. Kung – Pfizer, Incorporated, Groton, Connecticut 06340, United States; [orcid.org/0000-0002-5019-1939](https://orcid.org/0000-0002-5019-1939)

Yajing Lian – Pfizer, Incorporated, Groton, Connecticut 06340, United States

Monica M. Li – Pfizer, Incorporated, Cambridge, Massachusetts 02139, United States

Qifang Li – Pfizer, Incorporated, Groton, Connecticut 06340, United States

Luis A. Martinez-Alsina – Pfizer, Incorporated, Groton, Connecticut 06340, United States

Rebecca O'Connor – Pfizer, Incorporated, Groton, Connecticut 06340, United States

Kevin Ogilvie – Pfizer, Incorporated, Groton, Connecticut 06340, United States

Kiyoyuki Omoto – Pfizer, Incorporated, Cambridge, Massachusetts 02139, United States

Brian Raymer – Pfizer, Incorporated, Cambridge, Massachusetts 02139, United States

Matthew R. Reese – Pfizer, Incorporated, Groton, Connecticut 06340, United States

Tim Ryder – Pfizer, Incorporated, Groton, Connecticut 06340, United States

Lacey Samp – Pfizer, Incorporated, Groton, Connecticut 06340, United States

Kimberly A. Stevens – Pfizer, Incorporated, Groton, Connecticut 06340, United States

Daniel W. Widlicka – Pfizer, Incorporated, Groton, Connecticut 06340, United States; [orcid.org/0000-0001-9565-7619](https://orcid.org/0000-0001-9565-7619)

Qingyi Yang – Pfizer, Incorporated, Cambridge, Massachusetts 02139, United States; [orcid.org/0000-0001-5269-0494](https://orcid.org/0000-0001-5269-0494)

Kaicheng Zhu – Pfizer, Incorporated, Groton, Connecticut 06340, United States

Jean-Philippe Fortin – Pfizer, Incorporated, Cambridge, Massachusetts 02139, United States

Matthew F. Sammons — Pfizer, Incorporated, Cambridge, Massachusetts 02139, United States; [orcid.org/0000-0001-6472-0646](https://orcid.org/0000-0001-6472-0646)

Complete contact information is available at:

<https://pubs.acs.org/10.1021/acs.jmedchem.2c02012>

## Notes

The authors declare the following competing financial interest(s): All authors were employed by Pfizer, Inc. at the time this work was completed.

## ABBREVIATIONS USED

AgRP, agouti-related peptide;  $\alpha$ -MSH,  $\alpha$ -melanocyte stimulating hormone; AmPhos, di-*tert*-butyl(4-dimethylaminophenyl)-phosphine; BrettPhos, 2-(dicyclohexylphosphino)-3,6-dimethoxy-2',4',6'-triisopropyl-1,1'-biphenyl; PPh<sub>3</sub>, triphenylphosphine; CCDC, Cambridge Crystallographic Data Centre; CDI, carbonyldiimidazole; CHO, Chinese Hamster Ovary; dba, dibenzylideneacetone; DBDMH, 1,3-dibromo-5,5-dimethylhydantoin; DPPA, diphenylphosphoryl azide; dppf, 1,1'-ferrocenediyl-bis(diphenylphosphine); ER, efflux ratio; HATU, 1-[bis(dimethylamino)methylene]-1*H*-1,2,3-triazolo[4,5-*b*]-pyridinium 3-oxid hexafluorophosphate; hERG, human ether-a-go-go; hHEP, human hepatocyte; MC4R, melanocortin-4 receptor; mBCRP, murine breast cancer resistance protein; MDR, multidrug-resistance protein 1; POMC, pro-opiomelanocortin; PVH, paraventricular nucleus of the hypothalamus; RDC, residual dipolar coupling; RuPhos, 2-dicyclohexylphosphino-2',6'-diisopropoxybiphenyl; TDI, time-dependent inhibition; Xantphos, 4,5-bis(diphenylphosphino)-9,9-dimethylxanthene

## REFERENCES

- (1) Tao, Y. X. The melanocortin-4 receptor: physiology, pharmacology, and pathophysiology. *Endocr. Rev.* **2010**, *31* (4), 506–543.
- (2) Nijenhuis, W. A. J.; Oosterom, J.; Adan, R. A. H. AgRP(83–132) acts as an inverse agonist on the human-melanocortin-4 receptor. *Mol. Endocr.* **2001**, *15* (1), 164–171.
- (3) Haskell-Luevano, C.; Monck, E. K. Agouti-related protein functions as an inverse agonist at a constitutively active brain melanocortin-4 receptor. *Regulat. Pep.* **2001**, *99* (1), 1–7.
- (4) Tao, Y.-X. Molecular mechanisms of the neural melanocortin receptor dysfunction in severe early onset obesity. *Mol. Cell. Endocr.* **2005**, *239* (1), 1–14.
- (5) Govaerts, C.; Srinivasan, S.; Shapiro, A.; Zhang, S.; Picard, F.; Clement, K.; Lubrano-Berthelot, C.; Vaisse, C. Obesity-associated mutations in the melanocortin 4 receptor provide novel insights into its function. *Peptides* **2005**, *26* (10), 1909–1919.
- (6) Clark, A. J. L. 60 Years of POMC: the proopiomelanocortin gene: discovery, deletion and disease. *J. Mol. Endocr.* **2016**, *56* (4), T27–T37.
- (7) Krude, H.; Biebermann, H.; Gruters, A. Mutations in the human proopiomelanocortin gene. *Ann. N.Y. Acad. Sci.* **2003**, *994* (1), 233–239.
- (8) Krude, H.; Gruters, A. Implications of proopiomelanocortin (POMC) mutations in humans: The POMC deficiency syndrome. *Trends Endocr. Met.* **2000**, *11* (1), 15–22.
- (9) DeBoer, M. D.; Marks, D. L. Therapy insight: use of melanocortin antagonists in the treatment of cachexia in chronic disease. *Nat. Clin. Pract. Endocrinol. Metab.* **2006**, *2* (8), 459–466.
- (10) Ujjainwalla, F.; Sebat, I. K. Small molecule ligands of the human melanocortin-4 receptor. *Curr. Top. Med. Chem.* **2007**, *7* (11), 1068–1084.
- (11) Todorovic, A.; Haskell-Luevano, C. A review of melanocortin receptor small molecule ligands. *Peptides* **2005**, *26* (10), 2026–2036.

(12) Nozawa, D.; Chaki, S.; Nakazato, A. Recent advances in the development of melanocortin-4 receptor ligands. *Expert. Opin. Ther. Pat.* **2008**, *18* (4), 403–427.

(13) Ericson, M. D.; Lensing, C. J.; Fleming, K. A.; Schlasner, K. N.; Doering, S. R.; Haskell-Luevano, C. Bench-top to clinical therapies: A review of melanocortin ligands from 1954 to 2016. *Biochim. Biophys. Acta. Mol. Basis. Dis.* **2017**, *1863* (10), 2414–2435.

(14) Weyermann, P.; Dallmann, R.; Magyar, J.; Anklin, C.; Hufschmidt, M.; Dubach-Powell, J.; Courdier-Fruh, I.; Henneböhle, M.; Nordhoff, S.; Mondadori, C. Orally available selective melanocortin-4 receptor antagonists stimulate food intake and reduce cancer-induced cachexia in mice. *PLoS One* **2009**, *4* (3), e4774.

(15) Cole, P.; Vasiliou, S.; Mormeneo, D.; Rosa, E. Medicinal chemistry selections from the 237th American Chemical Society National Meeting & Exposition. *Drugs of the Future* **2009**, *34* (6), 509–520.

(16) Vos, T. J.; Caracoti, A.; Che, J. L.; Dai, M.; Farrer, C. A.; Forsyth, N. E.; Drabic, S. V.; Horlick, R. A.; Lamppu, D.; Yowe, D. L.; Balani, S.; Li, P.; Zeng, H.; Joseph, I. B. J. K.; Rodriguez, L. E.; Maguire, M. P.; Patane, M. A.; Claiborne, C. F. Identification of 2-{2-[2-(5-Bromo-2-methoxyphenyl)-ethyl]-3-fluorophenyl}-4,5-dihydro-1*H*-imidazole (ML00253764), a small molecule melanocortin 4 receptor antagonist that effectively reduces tumor-induced weight loss in a mouse model. *J. Med. Chem.* **2004**, *47* (7), 1602–1604.

(17) Markison, S.; Foster, A. C.; Chen, C.; Brookhart, G. B.; Hesse, A.; Hoare, S. R. J.; Fleck, B. A.; Brown, B. T.; Marks, D. L. The regulation of feeding and metabolic rate and the prevention of murine cancer cachexia with a small-molecule melanocortin-4 receptor antagonist. *Endocrinology* **2005**, *146* (6), 2766–2773.

(18) Tucci, F. C.; White, N. S.; Markison, S.; Joppa, M.; Tran, J. A.; Fleck, B. A.; Madan, A.; Dyck, B. P.; Parker, J.; Pontillo, J.; Melissa Arellano, L.; Marinkovic, D.; Jiang, W.; Chen, C. W.; Gogas, K. R.; Goodfellow, V. S.; Saunders, J.; Foster, A. C.; Chen, C. Potent and orally active non-peptide antagonists of the human melanocortin-4 receptor based on a series of trans-2-disubstituted cyclohexylpiperazines. *Bioorg. Med. Chem. Lett.* **2005**, *15* (19), 4389–4395.

(19) Zhu, X.; Callahan, M. F.; Gruber, K. A.; Szumowski, M.; Marks, D. L. Melanocortin-4 receptor antagonist TCMCB07 ameliorates cancer- and chronic kidney disease-associated cachexia. *J. Clin. Invest.* **2020**, *130* (9), 4921–4934.

(20) Axiak-Bechtel, S. M.; Leach, S. B.; Scholten, D. G.; Newton-Northup, J. R.; Johnson, B. J.; Durham, H. E.; Gruber, K. A.; Callahan, M. F. Pharmacokinetics and safety of TCMCB07, a melanocortin-4 antagonist peptide in dogs. *Pharmacol. Res. Perspect.* **2021**, *9* (3), No. e00777.

(21) Lansdell, M. I.; Hepworth, D.; Calabrese, A.; Brown, A. D.; Blagg, J.; Burring, D. J.; Wilson, P.; Fradet, D.; Brown, T. B.; Quinton, F.; Mistry, N.; Tang, K.; Mount, N.; Stacey, P.; Edmunds, N.; Adams, C.; Gaboardi, S.; Neal-Morgan, S.; Wayman, C.; Cole, S.; Phipps, J.; Lewis, M.; Verrier, H.; Gillon, V.; Feeder, N.; Heatherington, A.; Sultana, S.; Haughey, S.; Martin, S. W.; Sudworth, M.; Tweedy, S. Discovery of a Selective Small-Molecule Melanocortin-4 Receptor Agonist with Efficacy in a Pilot Study of Sexual Dysfunction in Humans. *J. Med. Chem.* **2010**, *53* (8), 3183–3197.

(22) Kenakin, T. Predicting therapeutic value in the lead optimization phase of drug discovery. *Nat. Rev. Drug Discovery* **2003**, *2* (6), 429–438.

(23) Anderson, D.; Bai, G.; Cabral, S.; Piotrowski, D. W.; Wei, L. N → N' acyl migration in the context of a medicinal chemistry program. *Tetrahedron* **2022**, *123*, 132950.

(24) Sawyer, T. K.; Sanfilippo, P. J.; Hraby, V. J.; Engel, M. H.; Heward, C. B.; Burnett, J. B.; Hadley, M. E. 4-Norleucine, 7-D-phenylalanine- $\alpha$ -melanocyte-stimulating hormone: a highly potent  $\alpha$ -melanotropin with ultralong biological activity. *Proc. Natl. Acad. Sci. U. S. A.* **1980**, *77* (10), 5754–5758.

(25) Conde-Frieboes, K.; Thøgersen, H.; Lau, J. F.; Sensfuss, U.; Hansen, T. K.; Christensen, L.; Spetzler, J.; Olsen, H. B.; Nilsson, C.; Raun, K.; Dahl, K.; Hansen, B. S.; Wulff, B. S. Identification and in vivo and in vitro characterization of long acting and melanocortin 4 receptor



- (MC4-R) selective  $\alpha$ -melanocyte-stimulating hormone ( $\alpha$ -MSH) analogues. *J. Med. Chem.* **2012**, *55* (5), 1969–1977.
- (26) Tseng, E.; Eng, H.; Lin, J.; Cerny, M. A.; Tess, D. A.; Goosen, T. C.; Obach, R. S. Static and dynamic projections of drug-drug interactions caused by cytochrome P450 3A time-dependent inhibitors measured in human liver microsomes and hepatocytes. *Drug Metab. Dispos.* **2021**, *49* (10), 947–960.
- (27) Shamovsky, I.; Connolly, S.; David, L.; Ivanova, S.; Nordén, B.; Springthorpe, B.; Urbahns, K. Overcoming undesirable hERG potency of chemokine receptor antagonists using baseline lipophilicity relationships. *J. Med. Chem.* **2008**, *51* (5), 1162–1178.
- (28) Keefer, C.; Chang, G.; Carlo, A.; Novak, J. J.; Banker, M.; Carey, J.; Cianfroga, J.; Eng, H.; Jagla, C.; Johnson, N.; Jones, R.; Jordan, S.; Lazzaro, S.; Liu, J.; Scott Obach, R.; Riccardi, K.; Tess, D.; Umland, J.; Racich, J.; Varma, M.; Visswanathan, R.; Di, L. Mechanistic insights on clearance and inhibition discordance between liver microsomes and hepatocytes when clearance in liver microsomes is higher than in hepatocytes. *Eur. J. Pharm. Sci.* **2020**, *155*, 105541.
- (29) Trapa, P. E.; Troutman, M. D.; Lau, T. Y.; Wager, T. T.; Maurer, T. S.; Patel, N. C.; West, M. A.; Umland, J. P.; Carlo, A. A.; Feng, B.; Liras, J. L. In vitro–in vivo extrapolation of key transporter activity at the blood–brain barrier. *Drug Metab. Dispos.* **2019**, *47* (4), 405–411.
- (30) Lombardo, F.; Shalaeva, M. Y.; Tupper, K. A.; Gao, F. ElogDoct: A tool for lipophilicity determination in drug discovery. 2. basic and neutral compounds. *J. Med. Chem.* **2001**, *44* (15), 2490–2497.
- (31) Lombardo, F.; Shalaeva, M. Y.; Tupper, K. A.; Gao, F.; Abraham, M. H. ElogPoc: A tool for lipophilicity determination in drug discovery. *J. Med. Chem.* **2000**, *43* (15), 2922–2928.
- (32) Feng, B.; West, M.; Patel, N. C.; Wager, T.; Hou, X.; Johnson, J.; Tremaine, L.; Liras, J. Validation of human MDRI-MDCK and BCRP-MDCK cell lines to improve the prediction of brain penetration. *J. Pharm. Sci.* **2019**, *108* (7), 2476–2483.
- (33) Stopher, D.; McClean, S. An improved method for the determination of distribution coefficients. *J. Pharm. Pharmacol.* **2011**, *42* (2), 144–144.
- (34) ConQuest 2.0.5; Cambridge Crystallographic Data Center Inc., 2020.
- (35) Farley, K. A.; Che, Y.; Navarro-Vázquez, A.; Limberakis, C.; Anderson, D.; Yan, J.; Shapiro, M.; Shanmugasundaram, V.; Gil, R. R. Cyclic peptide design guided by residual dipolar couplings, J-couplings, and intramolecular hydrogen bond analysis. *J. Org. Chem.* **2019**, *84* (8), 4803–4813.
- (36) Farley, K. A.; Koos, M. R. M.; Che, Y.; Horst, R.; Limberakis, C.; Bellenger, J.; Lira, R.; Gil-Silva, L. F.; Gil, R. R. Cross-linked poly-4-acrylomorpholine: a flexible and reversibly compressible aligning gel for anisotropic NMR analysis of peptides and small molecules in water. *Angew. Chem., Int. Ed.* **2021**, *60* (50), 26314–26319.
- (37) Horst, R.; Farley, K. A.; Kormos, B. L.; Withka, J. M. NMR spectroscopy: the swiss army knife of drug discovery. *J. Biomol. NMR* **2020**, *74* (10), 509–519.
- (38) Protein database; <https://www.wwpdb.org/> (accessed 04–22–22).
- (39) Di, L.; Whitney-Pickett, C.; Umland, J. P.; Zhang, H.; Zhang, X.; Gebhard, D. F.; Lai, Y.; Federico, J. J.; Davidson, R. E.; Smith, R.; Reyner, E. L.; Lee, C.; Feng, B.; Rotter, C.; Varma, M. V.; Kempshall, S.; Fenner, K.; El-kattan, A. F.; Liston, T. E.; Troutman, M. D. Development of a new permeability assay using low-efflux MDCKII cells. *J. Pharm. Sci.* **2011**, *100* (11), 4974–4985.
- (40) Chen, Q.-Y.; Wu, S.-W. Methyl fluorosulphonyldifluoroacetate; a new trifluoromethylating agent. *J. Chem. Soc., Chem. Commun.* **1989**, No. 11, 705–706.
- (41) Molander, G. A.; Cavalcanti, L. N.; García-García, C. Nickel-catalyzed borylation of halides and pseudohalides with tetrahydroxydiboron [B<sub>2</sub>(OH)<sub>4</sub>]. *J. Org. Chem.* **2013**, *78* (13), 6427–6439.
- (42) Heller, S. T.; Fu, T.; Sarpong, R. Dual brønsted acid/nucleophilic activation of carbonylimidazole derivatives. *Org. Lett.* **2012**, *14* (8), 1970–1973.
- (43) World Press Enzymes. [https://wordpress.enzymicals.com/wp-content/uploads/2021/12/enzymicals\\_portfolio\\_2021\\_04\\_16.pdf](https://wordpress.enzymicals.com/wp-content/uploads/2021/12/enzymicals_portfolio_2021_04_16.pdf) (accessed 11–23–22).
- (44) Gao, Y.; Sharpless, K. B. Vicinal diol cyclic sulfates. Like epoxides only more reactive. *J. Am. Chem. Soc.* **1988**, *110* (22), 7538–7539.
- (45) Bower, J. F.; Szeto, P.; Gallagher, T. Enantiopure 1,4-Benzoxazines via 1,2-Cyclic Sulfamidates. Synthesis of Levofloxacin. *Org. Lett.* **2007**, *9* (17), 3283–3286.
- (46) Sengupta, P. The laboratory rat: relating its age with human's. *Int. J. Prev. Med.* **2013**, *4* (6), 624–630.
- (47) Santulli, G.; Borrás, C.; Bousquet, J.; Calza, L.; Cano, A.; Illario, M.; Franceschi, C.; Liotta, G.; Maggio, M.; Molloy, W. D.; Montuori, N.; O'Caomh, R.; Orfila, F.; Rauter, A. P.; Santoro, A.; Iaccarino, G. Models for preclinical studies in aging-related disorders: One is not for all. *Transl. Med. Unisa* **2015**, *13*, 4–12.
- (48) Ibebunjo, C.; Chick, J. M.; Kendall, T.; Eash, J. K.; Li, C.; Zhang, Y.; Vickers, C.; Wu, Z.; Clarke, B. A.; Shi, J.; Cruz, J.; Fournier, B.; Brachat, S.; Gutzwiller, S.; Ma, Q.; Markovits, J.; Broome, M.; Steinkrauss, M.; Skuba, E.; Galarneau, J.-R.; Gygi, S. P.; Glass, D. J. Genomic and proteomic profiling reveals reduced mitochondrial function and disruption of the neuromuscular junction driving rat sarcopenia. *Mol. Cell. Biol.* **2013**, *33* (2), 194–212.
- (49) Altun, M.; Bergman, E.; Edstrom, E.; Johnson, H.; Ulfhake, B. Behavioral impairments of the aging rat. *Physiol. Behav.* **2007**, *92* (5), 911–923.
- (50) Nistiar, F.; Racz, O.; Lukacinova, A.; Hubkova, B.; Novakova, J.; Lovasova, E.; Sedlakova, E. Age dependency on some physiological and biochemical parameters of male Wistar rats in controlled environment. *J. Environ. Sci. Heal. A* **2012**, *47* (9), 1224–1233.
- (51) Envigo Study C11963 Model Development.
- (52) Landi, F.; Calvani, R.; Tosato, M.; Martone, A. M.; Ortolani, E.; Saveria, G.; Sisto, A.; Marzetti, E. Anorexia of aging: risk factors, consequences, and potential treatments. *Nutrients* **2016**, *8* (2), 69.
- (53) Tsutsumimoto, K.; Doi, T.; Makizako, H.; Hotta, R.; Nakakubo, S.; Makino, K.; Suzuki, T.; Shimada, H. The association between anorexia of aging and physical frailty: Results from the national center for geriatrics and gerontology's study of geriatric syndromes. *Maturitas* **2017**, *97*, 32–37.
- (54) Tsutsumimoto, K.; Doi, T.; Makizako, H.; Hotta, R.; Nakakubo, S.; Makino, K.; Suzuki, T.; Shimada, H. Aging-related anorexia and its association with disability and frailty. *J. Cachexia Sarcopenia* **2018**, *9* (5), 834–843.
- (55) Roy, M.; Gaudreau, P.; Payette, H. A scoping review of anorexia of aging correlates and their relevance to population health interventions. *Appetite* **2016**, *105*, 688–699.
- (56) Wolden-Hanson, T. Mechanisms of the anorexia of aging in the Brown Norway rat. *Physiol. Behav.* **2006**, *88* (3), 267–276.
- (57) Furedi, N.; Miko, A.; Gaszner, B.; Feller, D.; Rostas, I.; Tenk, J.; Solymar, M.; Balasko, M.; Petervari, E. Activity of the hypothalamic melanocortin system decreases in middle-aged and increases in old rats. *J. Gerontol. a-Biol.* **2018**, *73* (4), 438–445.
- (58) Petervari, E.; Garami, A.; Soos, S.; Szekely, M.; Balasko, M. Age-dependence of alpha-MSH-induced anorexia. *Neuropeptides* **2010**, *44* (4), 315–322.
- (59) Petervari, E.; Szabad, A. O.; Soos, S.; Garami, A.; Szekely, M.; Balasko, M. Central alpha-MSH infusion in rats: Disparate anorexic vs. metabolic changes with aging. *Regulat. Pep.* **2011**, *166* (1–3), 105–111.
- (60) Wolden-Hanson, T.; Marck, B. T.; Matsumoto, A. M. Blunted hypothalamic neuropeptide gene expression in response to fasting, but preservation of feeding responses to AgRP in aging male Brown Norway rats. *Am. J. Physiol.-Reg. I* **2004**, *287* (1), R138–R146.
- (61) Wysokinski, A.; Sobow, T.; Kloszewska, I.; Kostka, T. Mechanisms of the anorexia of aging—a review. *Age* **2015**, *37* (4), 81.
- (62) Uniprot; <https://www.uniprot.org/uniprot/Q4JIV8> (accessed 11–11–22).
- (63) Uniprot; <https://www.uniprot.org/uniprot/P32245/entry> (accessed 11–23–22).



(64) Clinicaltrials.gov; <https://clinicaltrials.gov/ct2/results?cond=&term=PF-07258669&cntry=&state=&city=&dist=> (accessed 11–23–22).